

A TETRAHEDRAL SPACE-FILLING CURVE FOR NON-CONFORMING ADAPTIVE MESHES

CARSTEN BURSTEDDE* AND JOHANNES HOLKE*

Abstract. We introduce a space-filling curve for triangular and tetrahedral red-refinement that can be computed using bitwise interleaving operations similar to the well-known Z-order or Morton curve for cubical meshes. To store the information necessary for random access, we suggest 10 bytes per triangle and 14 bytes per tetrahedron. We present algorithms that compute the parent, children, and face-neighbors of a mesh element in constant time, as well as the next and previous element in the space-filling curve and whether a given element is on the boundary of the root simplex or not. Furthermore, we prove that the maximum number of face-connected components in any segment of this curve is bounded by twice the refinement level plus one (minus one in 2d) and that the number of corner-connected components is bounded by two. We conclude with a scalability demonstration that creates and adapts selected meshes on a large distributed-memory system.

Key words. Forest of octrees, parallel adaptive mesh refinement, Morton code, high performance computing, non-conforming simplicial mesh, space-filling curve

AMS subject classifications. 65M50, 68W10, 65Y05, 65D18

1. Introduction. Conforming adaptive mesh refinement for simplicial (triangular and tetrahedral) meshes is one of the most successful concepts in numerical mathematics and computational science and engineering; see e.g. [3, 18, 44]. Simplices provide high flexibility in meshing to arbitrary domain geometries [40, 41] and can be mapped using an element-wise constant Jacobian in most cases, which allows for an efficient numerical implementation. Discretization and integration methods of various kinds are available for both low and high orders of accuracy.

Large-scale scientific computing incurs the additional requirements of (1) fast and scalable algorithms for adaptive refinement and coarsening (AMR) as well as (2) parallel partitioning. One class of methods for AMR exploits the properties of Delaunay triangulations [20, 22, 39], while partitioning of unstructured meshes is often approached by formulating the mesh topology as a graph. Common application codes such as FEniCS [27], PLUM [29, 30], OpenFOAM [31] or MOAB from the SIGMA toolkit [47] delegate graph partitioning to third-party software like ParMETIS [24] or Scotch [17]. These methods have been improved considerably in the limit of millions of processors and billions of elements [15, 36, 43]. Still, increasing the scalability and decreasing the absolute runtime and memory demands of in-situ implementations remains a challenge, and the lack of an obvious hierarchy prevents certain use cases.

Non-conforming AMR in combination with recursive refinement, on the other hand, makes refinement and coarsening near-trivial operations. The additional mathematical logic to enable hanging faces and edges is by now well understood for both continuous and discontinuous discretizations [1, 19, 37]. The resolution may be as coarse as any chosen root mesh, which poses only a slight limit to geometric flexibility. The second challenge, namely the partitioning of meshes, may be approached using space-filling curves (SFC). Instead of working on the NP-hard graph partitioning problem [11], SFCs are used to approximately solve the partitioning problem in linear runtime [4, 51]. The Sierpinski curve [42] and generalized versions of it are the most common space-filling curves on simplicial meshes. These were described by Bänsch [7],

*Institut für Numerische Simulation (INS) and Hausdorff Center for Mathematics (HCM), Rheinische Friedrich-Wilhelms-Universität Bonn, Germany

Kossaczky [25], and others; see e.g. [4, 38].

When using hypercubes as mesh primitives, the SFC logic simplifies greatly due to the tensor product structure [33, 45, 46, 48, 51]. It is also well-suited to compute topological entities like face-neighbors, children, and parents of given mesh elements while being memory efficient as well. This is due to the fact that for a mesh element only the coordinates of one anchor node plus its refinement level have to be stored. Today, this principle has found its way into widely used software libraries [5, 6]. Memory usage can be further optimized by incremental encoding along the SFC [4, 49].

Using SFCs on hexahedral meshes is exceptionally fast and scalable [12, 23, 35], which even allows it to be used to partition simplices by mapping them into a surrounding cube [2]. Yet, hexahedral AMR is more limited geometrically than simplicial AMR. Thus, in this paper, we attempt a synthesis by establishing a space filling curve for triangles and tetrahedra that has many of the favorable properties known for hexahedra.

Our starting point is to divide the simplices in a refined mesh into two (2D) respectively six (3D) different types and selecting for each type a specific ordering for Beys' red-refinement [8]. This type and the coordinates of one vertex of a simplex serve as a unique identifier, the Tet-id, of the simplex in question. We then propose a Morton-type coordinate mapping that can be computed from the Tet-id and gives rise to a SFC. Based on this logic, we develop level-independent constant-time algorithms to compute the tetrahedral-Morton identifiers of any parent, child, face-neighbor, SFC-successor and -predecessor and to decide whether for two given elements one is an ancestor of the other. We prove properties of the (face-)continuity of the SFC and conclude with scalability tests of mesh creation and adaptation with over 8.5×10^{11} tetrahedral mesh elements on up to 131,072 cores of the JUQUEEN supercomputer and 786,432 cores of the MIRA supercomputer.

2. Bey's refinement rule. Our aim is to define and examine a new space-filling curve for the non-conforming Bey-refinement (also called red-refinement) patterns of triangles and tetrahedra [8, 9, 50], which we briefly repeat in this section. We refer to triangles and tetrahedra as d -simplices, where $d \in \{2, 3\}$ specifies the dimension. It is sometimes convenient to drop d from this notation. A d -simplex $T \subseteq \mathbb{R}^d$ is uniquely determined by its $d + 1$ affine-independent corner nodes $x_0, \dots, x_d \in \mathbb{R}^d$, whose order will be significant for the refinement rule. Therefore, we write

$$T = [x_0, x_1, x_2] \quad \text{in 2D and} \quad (2.1a)$$

$$T = [x_0, x_1, x_2, x_3] \quad \text{in 3D.} \quad (2.1b)$$

Define x_0 as the *anchor node* of T . The notation x_{ij} will denote the midpoint between x_i and x_j , thus $x_{ij} = \frac{1}{2}(x_i + x_j)$.

Definition 1. Given a d -simplex $T = [x_0, \dots, x_d] \subset \mathbb{R}^d$, the refinement rule of Bey consists of cutting off four subtetrahedra at the corners (as in Figure 2.1). In 3D the remaining octahedron is then divided along the diagonal from x_{02} to x_{13} . Bey numbers the 2^d resulting subsimplices as follows.

$$d = 2 : \quad \begin{array}{ll} T_0 & := [x_0, x_{01}, x_{02}], & T_1 & := [x_{01}, x_1, x_{12}], \\ T_2 & := [x_{02}, x_{12}, x_2], & T_3 & := [x_{01}, x_{02}, x_{12}], \end{array} \quad (2.2a)$$

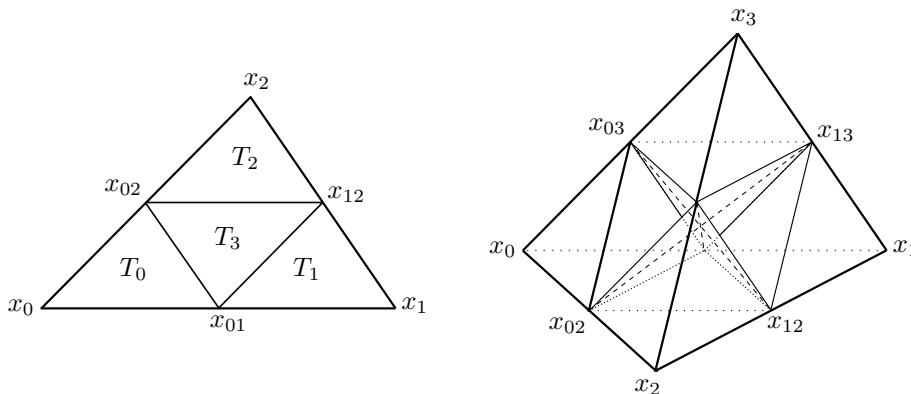


FIGURE 2.1. *Left: The refinement scheme for triangles in two dimensions. A triangle $T = [x_0, x_1, x_2] \subset \mathbb{R}^2$ is refined by dividing each face at the midpoints x_{ij} . We obtain four smaller triangles, all similar to T . Right: The situation in three dimensions. If we divide the edges of the tetrahedron $T = [x_0, x_1, x_2, x_3] \subset \mathbb{R}^3$ in half, we get four smaller tetrahedra (similar to T) and one octahedron. By dividing the inner octahedron along any of its three diagonals (shown dashed) we finally end up with a partition of T into eight smaller tetrahedra, all having the same volume. The refinement rule of Bey is obtained by always choosing the diagonal from x_{02} to x_{13} and numbering the corners of the children according to (2.2).*

$$\begin{aligned}
 d = 3 : \quad & T_0 := [x_0, x_{01}, x_{02}, x_{03}], & T_4 &:= [x_{01}, x_{02}, x_{03}, x_{13}], \\
 & T_1 := [x_{01}, x_1, x_{12}, x_{13}], & T_5 &:= [x_{01}, x_{02}, x_{12}, x_{13}], \\
 & T_2 := [x_{02}, x_{12}, x_2, x_{23}], & T_6 &:= [x_{02}, x_{03}, x_{13}, x_{23}], \\
 & T_3 := [x_{03}, x_{13}, x_{23}, x_3], & T_7 &:= [x_{02}, x_{12}, x_{13}, x_{23}].
 \end{aligned} \tag{2.2b}$$

Definition 2. In this paper, a *refinement* of a d -simplex S denotes a set \mathcal{S} of d -dimensional subsimplices of S that can be constructed from the following two rules:

- $\mathcal{S} = \{S\}$ is a refinement of S .
- If \mathcal{S} is a refinement of S then $\mathcal{S}' = (\mathcal{S} \setminus \{T\}) \cup \{T_0, \dots, T_{2^d-1}\}$ is a refinement for every $T \in \mathcal{S}$. This rule amounts to refining the simplex T .

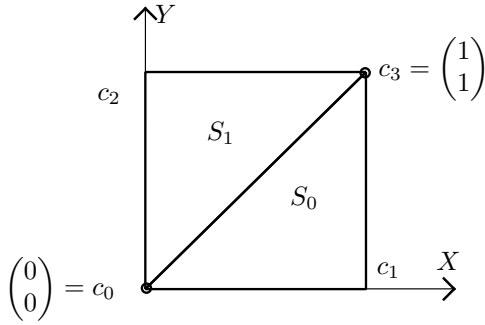
We explicitly allow nonuniform refinements and thus non-conforming faces and edges.

Definition 3. The T_i from (2.2) are called the *children* of T and T is called *parent* of the T_i , written $T = P(T_i)$. Therefore, we also call the T_i *siblings* of each other. If a d -simplex T belongs to a refinement of another d -simplex S , then T is a *descendant* of S and S is an *ancestor* of T . The number ℓ of refining steps needed to obtain T from S is unique and called the *level* of T (w.r.t. S); we write $\ell = \ell(T)$. Usually S is clear from the context and therefore omitted in the notation. By definition, T is an ancestor and descendant of itself.

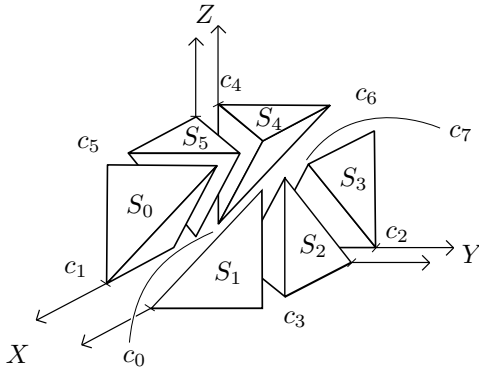
Consider the six tetrahedra $S_0, \dots, S_5 \subset \mathbb{R}^3$ given in Figure 2.2. These tetrahedra form a triangulation of the unit cube. The results and algorithms in this paper rely on the following property [8]:

Property 1. Refining the six tetrahedra from the triangulation of the unit cube simultaneously to level ℓ results in the same mesh as first refining the unit cube to level ℓ and then triangulating each smaller cube with the six tetrahedra S_0, \dots, S_5 , scaled by a factor of $2^{-\ell}$ (see Figure 2.3). The same behaviour occurs in two dimensions when the unit square is divided into two triangles.

3. A tetrahedral Morton index. The Morton index or Z-order for a cube in a hexahedral mesh is computed by bitwise interleaving the coordinates of the anchor



2D	x_0	x_1	x_2
S_0	c_0	c_1	c_3
S_1	c_0	c_2	c_3

(2.3a)


3D	x_0	x_1	x_2	x_3
S_0	c_0	c_1	c_5	c_7
S_1	c_0	c_1	c_3	c_7
S_2	c_0	c_2	c_3	c_7
S_3	c_0	c_2	c_6	c_7
S_4	c_0	c_4	c_6	c_7
S_5	c_0	c_4	c_5	c_7

(2.3b)

FIGURE 2.2. The basic triangle (2D) and tetrahedra types (3D) obtained by dividing $[0, 1]^d$. Top Left: The unit square can be divided into two triangles sharing the edge from $(0, 0)^t$ to $(1, 1)^t$. We denote these triangles by S_0 and S_1 . The four corners of the square are numbered c_0, \dots, c_3 in yx -order. Top Right: The corner nodes of S_0 and S_1 in terms of the square corners. Bottom Left (exploded view): In three dimensions the unit cube can be divided into six tetrahedra, all sharing the edge from the origin to $(1, 1, 1)^t$. We denote these tetrahedra by S_0, \dots, S_5 . The eight corners of the cube are numbered c_0, \dots, c_7 in zyx -order (Redrawn and modified with permission [8]). Bottom Right: The corner nodes of the six tetrahedra S_0, \dots, S_5 in terms of the cube corners.

node of the cube [28]. In this section we present an index for d -simplices that also uses the bitwise interleaving approach, the tetrahedral Morton index or TM-index. To define the TM-index we look at refinements of a reference simplex, which we define in Section 3.1 below. For each d -simplex in a refinement of the reference simplex we define a unique identifier, the so called Tet-id, which serves as the input to compute the TM-index and for all algorithms related to it. This Tet-id consists of the coordinates of the anchor node of the considered simplex plus one additional number, the type of the simplex. We define the Tet-id and type in Section 3.2. We then define the TM-index in Section 3.3 and in the following subsections we show that it possesses locality properties similar to those of the Morton index.

3.1. The reference simplex. Throughout the rest of this paper, let \mathcal{L} be a given maximal refinement level. Instead of the unit cube $[0, 1]^d$, we consider the scaled cube $[0, 2^{\mathcal{L}}]^d$, ensuring that all node coordinates in a refinement up to level \mathcal{L} are integers. Suppose we are given some d -simplex $T \subset \mathbb{R}^d$ together with a refinement \mathcal{S} of T . By mapping T affine-linearly to $2^{\mathcal{L}} * S_0$ the refinement \mathcal{S} is mapped to a refinement \mathcal{S}' of $2^{\mathcal{L}} * S_0$. Therefore, to examine space-filling curves on refinements

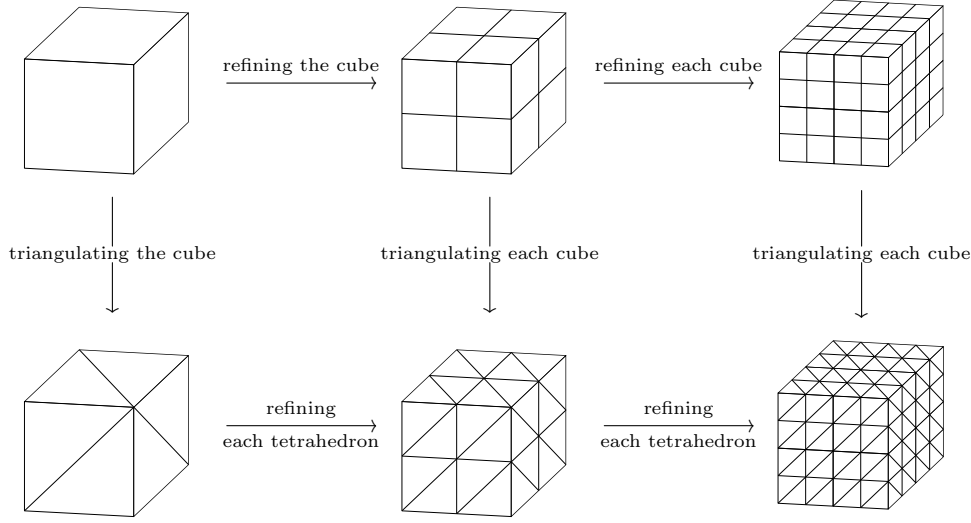


FIGURE 2.3. Triangulating a cube according to Figure 2.2 and then refining the tetrahedra via Bey's refinement rule results in the same mesh as first refining the cube into eight subcubes and afterwards triangulating each of these cubes. Each occurring tetrahedron is uniquely determined by the subcube it lies in plus its type. The same situation can be observed in two dimensions if we restrict our view to one side of the cube.

of T , it suffices to examine space-filling curves on $2^\mathcal{L} * S_0$. So from now on we only consider refinements of the d -simplex $T_d^0 := 2^\mathcal{L} * S_0$. Let \mathcal{T}_d be the set of all possible descendants of this d -simplex with level smaller or equal to \mathcal{L} , thus

$$\mathcal{T}_d = \{ T \mid T \text{ is a descendant of } T_d^0 \text{ with } 0 \leq \ell(T) \leq \mathcal{L} \}. \quad (3.1)$$

Any refinement (up to level \mathcal{L}) of T_d^0 is a subset of \mathcal{T}_d , and for each $T \in \mathcal{T}_d$ there exists at least one refinement \mathcal{S} of T_d^0 with $T \in \mathcal{S}$. In this context, we will refer to T_d^0 as the *root simplex*. Furthermore, let \mathbb{L}^d denote the set of all possible anchor node coordinates of d -simplices in \mathcal{T}_d , thus

$$\begin{aligned} \mathbb{L}^2 &= \{ [0, 2^\mathcal{L}]^2 \cap \mathbb{Z}^2 \mid y \leq x \}, \\ \mathbb{L}^3 &= \{ [0, 2^\mathcal{L}]^3 \cap \mathbb{Z}^3 \mid y \leq z \leq x \}. \end{aligned} \quad (3.2)$$

Note that we could have chosen any other of the S_i (scaled by $2^\mathcal{L}$) as the root simplex and we do not see any advantage or disadvantage in doing so.

3.2. The type and Tet-id of a d -simplex. Making use of Property 1, we formulate

Definition 4. Each d -simplex $T \in \mathcal{T}_d$ of level ℓ lies in a d -cube of the hexahedral mesh that is part of a uniform level ℓ refinement of $[0, 2^\mathcal{L}]^d$. This specific cube is the *associated cube* of T and denoted by Q_T . The d -simplex T is a scaled and shifted version of exactly one of the six tetrahedra S_i that constitute the unit cube, and we define the *type* of T as this number, $\text{type}(T) := i$.

The anchor node of a subcube of level ℓ is the particular corner of that cube with the smallest x, y (and z) coordinates. This means that for each simplex T in the refinement from Figure 2.3 the anchor node of T and the anchor node of its

Ct	Child				Ct	Child					
	2D	T_0	T_1	T_2		T_3	3D	$T_0 \dots T_3$	T_4	T_5	T_6
b	0	0	0	0	1	0	0	4	5	2	1
	1	1	1	1	0	1	1	3	2	5	0
b	2	2	0	1	4	3	2	0	1	4	3
	3	3	5	4	1	2	3	0	5		
	4	4	2	3	0	5					
	5	5	1	0	3	4					

TABLE 3.1

For a d -simplex T of type b the table gives the types $Ct(T_0), \dots, Ct(T_{2^d-1})$ of T 's children. The corner-children T_0, T_1, T_2 (and in 3D also T_3) always have the same type as T .

associated cube coincide. Any two d -simplices in \mathcal{T}_d with the same associated cube are distinguishable by their type.

From Bey's observation from Figure 2.3 it follows that any simplex in \mathcal{T}_d can be obtained by specifying a level ℓ , then choosing one level ℓ subcube of the root cube and finally fixing a type. This consideration motivates the following definition.

Definition 5 (Tet-id). For $T = [x_0, \dots, x_d] \in \mathcal{T}_d$ we define the *Tet-id* of T as the tuple of its anchor node and type, thus

$$\text{Tet-id}(T) := (x_0, \text{type}(T)). \quad (3.3)$$

Lemma 6. Let $T, T' \in \mathcal{T}_d$ then $T = T'$ if and only if their *Tet-ids* and levels are the same.

Since any simplex in \mathcal{T}_d can be specified by the Tet-id and level, the Tet-id provides an important tool for our work. The construction of the tetrahedral Morton index in the next section and the algorithms that we present in Section 5 rely on the Tet-id as the fundamental data of a simplex. All information about a mesh can be extracted from the Tet-id and level of each element.

Let us shortly examine the distribution of the different types occurring in a uniform refinement of \mathcal{T}_d^0 . It is obvious that more simplices will have type 0 than any other type. However, a close examination of Table 3.1 together with a short inductive argument leads to

Proposition 7. In the limit $\ell \rightarrow \infty$ the different types of simplices in a uniform level ℓ refinement of \mathcal{T}_d occur in equal ratios.

3.3. Encoding of the tetrahedral Morton index. In addition to the anchor coordinates the tetrahedral Morton index also depends on the types of all ancestors of a simplex. In Section 5 we show that these information can be constructed from the Tet-id and level. We start by giving a formal definition of the interleaving operation and the additional information needed.

Definition 8. We define the *interleaving* $a \dot{\perp} b$ of two n -tuples $a = (a_{n-1}, \dots, a_0)$ and $b = (b_{n-1}, \dots, b_0)$ as the $2n$ -tuple obtained by alternating the entries of a and b :

$$a \dot{\perp} b := (a_{n-1}, b_{n-1}, \dots, a_0, b_0). \quad (3.4)$$

The interleaving of more than two n -tuples a^1, \dots, a^m is defined analogously as the mn -tuple

$$a^1 \dot{\perp} \dots \dot{\perp} a^m := (a_{n-1}^1, a_{n-1}^2, \dots, a_{n-1}^m, a_{n-2}^1, \dots, a_{n-2}^m, \dots, a_0^{m-1}, a_0^m). \quad (3.5)$$

The tetrahedral Morton index of a d -simplex $T \in \mathcal{T}_d$ that we are going to define will be the interleaving of $d + 1$ \mathcal{L} -tuples. The first d are the binary representations of the coordinates of T 's anchor node and the last is the tuple consisting of the types of the ancestors of T .

Definition 9. Let $T \in \mathcal{T}_3$ be a tetrahedron of refinement level ℓ with anchor node $x_0 = (x, y, z) \in \mathbb{L}^3$. Since $x, y, z \in \mathbb{N}_0$ with $0 \leq x, y, z < 2^\mathcal{L}$, we can express them as binary numbers with \mathcal{L} digits, writing

$$x = \sum_{j=0}^{\mathcal{L}-1} x_j 2^j, \quad y = \sum_{j=0}^{\mathcal{L}-1} y_j 2^j, \quad z = \sum_{j=0}^{\mathcal{L}-1} z_j 2^j. \quad (3.6)$$

We define the \mathcal{L} -tuples X, Y and Z as the \mathcal{L} -tuples consisting of the binary digits of x, y and z ; thus,

$$X = X(T) := (x_{\mathcal{L}-1}, \dots, x_0), \quad (3.7a)$$

$$Y = Y(T) := (y_{\mathcal{L}-1}, \dots, y_0), \quad (3.7b)$$

$$Z = Z(T) := (z_{\mathcal{L}-1}, \dots, z_0). \quad (3.7c)$$

For $d = 2$ we get the same definitions with X and Y , leaving out the z -coordinate.

Definition 10. For a $T \in \mathcal{T}_d$ of level ℓ and each $0 \leq j \leq \ell$ let T^j be the (unique) ancestor of T of level j . In particular, $T^\ell = T$. We define $B(T)$ as the \mathcal{L} -tuple consisting of the types of T 's ancestors in the first ℓ entries, starting with T^1 . The last $\mathcal{L} - \ell$ entries of $B(T)$ are zero.

$$B = B(T) := \left(\underbrace{\text{type}(T^1), \text{type}(T^2), \dots, \text{type}(T)}_{\ell \text{ entries}}, 0, \dots, 0 \right), \quad (3.8)$$

Thus, if we write B as an \mathcal{L} -tuple with indexed entries b_i

$$B = B(T) = (b_{\mathcal{L}-1}, \dots, b_0) \in \{0, \dots, d! - 1\}^\mathcal{L}, \quad (3.9)$$

then the i -th entry b_i is given as

$$b_i = \begin{cases} \text{type}(T^{\mathcal{L}-i}) & \mathcal{L} - 1 \geq i \geq \mathcal{L} - \ell, \\ 0 & \mathcal{L} - \ell > i \geq 0. \end{cases} \quad (3.10)$$

Definition 11 (tetrahedral Morton Index). We define the *tetrahedral Morton index* (*TM-index*) $m(T)$ of a d -simplex $T \in \mathcal{T}_d$ as the interleaving of the \mathcal{L} -tuples $(Z,)Y, X$ and B . Thus,

$$m(T) := Y \dot{\perp} X \dot{\perp} B \quad (3.11a)$$

for triangles and

$$m(T) := Z \dot{\perp} Y \dot{\perp} X \dot{\perp} B \quad (3.11b)$$

for tetrahedra.

This index resembles the well-known Morton index or Z-order for d -dimensional cubes, which we denote by \tilde{m} here. For such a cube Q the Morton index is usually defined as the bitwise interleaving of its coordinates, thus $\tilde{m}(Q) = Z \dot{\perp} Y \dot{\perp} X$ resp. $\tilde{m}(Q) = Y \dot{\perp} X$, see [14, 28, 46].

As we show in Section 5, the TM-index can be computed from the Tet-id of T with no further information given. Thus, in an implementation it is not necessary to store the \mathcal{L} -tuple B .

The TM-index of a d -simplex builds up from packs of d bits (z_i, y_i) and x_i followed by a type $b_i \in \{0, \dots, d! - 1\}$. Since $d! = 2 < 4$ for $d = 2$, we can interpret the two-dimensional TM-index as a quaternary number with digits $(y_i x_i)_2$ and b_i :

$$\begin{aligned} m(T) &= ((y_{\mathcal{L}-1} x_{\mathcal{L}-1})_2, b_{\mathcal{L}-1}, \dots, (y_0 x_0)_2, b_0)_4 \\ &= \sum_{i=0}^{\mathcal{L}} ((2y_i + x_i)4^{2i+1} + b_i 4^{2i}). \end{aligned} \quad (3.12a)$$

Similar, as an octal number with digits $(z_i y_i x_i)_2$ and b_i for $d = 3$, since then $d! = 6 < 8$.

$$\begin{aligned} m(T) &= ((z_{\mathcal{L}-1} y_{\mathcal{L}-1} x_{\mathcal{L}-1})_2, b_{\mathcal{L}-1}, \dots, (z_0 y_0 x_0)_2, b_0)_8 \\ &= \sum_{i=0}^{\mathcal{L}} ((4z_i + 2y_i + x_i)8^{2i+1} + b_i 8^{2i}). \end{aligned} \quad (3.12b)$$

The entries in these numbers are only nonzero up to the level ℓ of T , since $x_{\mathcal{L}-i} = y_{\mathcal{L}-i} = (z_{\mathcal{L}-i} =) b_{\mathcal{L}-i} = 0$ for all $i > \ell$. The octal/quaternary representation (3.12) directly gives an order on the TM-indices and therefore it is possible to construct a space-filling curve (SFC) from it, which we will examine further in Section 4. We use $m(T)$ to denote both the $(d+1)\mathcal{L}$ -tuple from (3.11) and the number given by (3.12).

Let us look at Figure 3.1 for a short example to motivate this definition of the TM-index. Since the anchor coordinates and the type together with the level uniquely determine a d -simplex in \mathcal{T}_d , one could ask why we do not define the index to be $((Z \perp) Y \perp X, \text{type}(T))$, a pair consisting of the Morton index of the associated cube of T and the type of T . This index was introduced for triangles in a slightly modified version as semi-quadcodes in [32] and would certainly require less information since the computation of the sequence B would not be necessary. However, it results in a SFC that traverses the leaf cubes of a refinement in the usual Z-order and inside of each cube it traverses the $d!$ different simplices in the order $S_0, \dots, S_{d!-1}$. As a result, there can be simplices T whose children are not traversed as a group, which means that there is a tetrahedron T' , which is not an ancestor or descendant of T , such that some child T_i of T is traversed before T' and T' is traversed before another child T_j of T . Theorem 14 states that this problem does not occur with the TM-index that we have defined above. Figure 3.1 compares the two approaches for a uniform level 2 refinement of T_2^0 .

3.4. A different approach to the TM-index. There is another interpretation of the TM-index, which is particularly useful for the AMR algorithms presented in Section 5. In order to define it we introduce the concept of the so called cube-id. According to Figure 2.2 we number the 2^d corners of a d -dimensional cube by c_0, \dots, c_{2^d-1} in a zyx -order (x varies fastest). When refining a cube to 2^d children, each child has exactly one of the c_i as a corner, and it is therefore convenient to number the children by c_0, \dots, c_{2^d-1} as well. For the child c_i we call the number i the *cube-id* of that child, see Figure 3.2 for an illustration. Since each cube Q that is not the root has a unique parent, it also has a unique cube-id. This cube-id can easily be computed by interleaving the last significant bits of the (z, y) and x coordinates of Q 's anchor node.

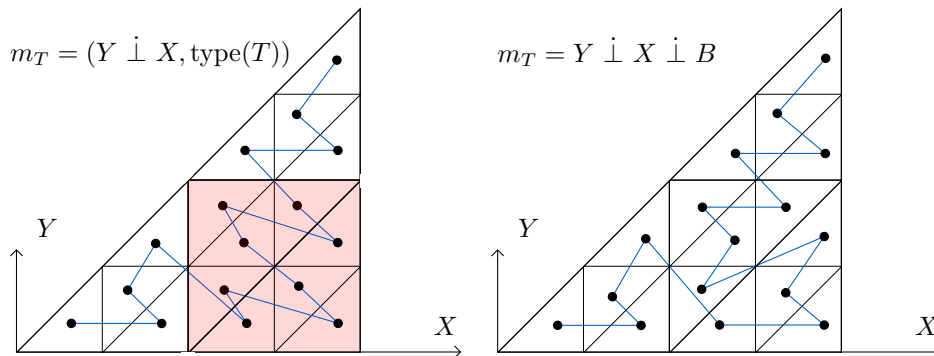


FIGURE 3.1. Two examples of space-filling curves (SFC) on a uniform level 2 refinement of T_2^0 . Left: The SFC arising if we choose $(Y \perp X, \text{type}(T))$ as index. As we see on the two coarse triangles that are shaded, the children of a level 1 triangle are not necessarily traversed before any other triangle is traversed. Such a locality property would be desirable, therefore this index is not suitable for our purposes. Right: The SFC arising from the TM-index from our Definition 11. We see that for each level 1 triangle its four children are traversed as a group. Theorem 14 states that this property holds for any parent triangle/tetrahedron. The order in which the children are traversed depends (only) on the type of the parent and is different from Bey's order given by (2.2).

Definition 12. Because each d -simplex $T \in \mathcal{T}_d$ of level ℓ has a unique associated cube we define the *cube-id* of T to be the cube-id of the associated cube of T , that is, the d -cube of level ℓ that has the same anchor node as T .

If X, Y (and Z) are as is in Definition 9 then we can write the cube-id of T 's ancestors as

$$\begin{aligned} \text{cube-id}(T^i) &= (y_i x_i)_2, & d = 2, \\ \text{cube-id}(T^i) &= (z_i y_i x_i)_2, & d = 3, \end{aligned} \quad (3.13)$$

and therefore using (3.12) we can rewrite the TM-index of T as

$$m(T) = (\text{cube-id}(T^1), \text{type}(T^1), \dots, \text{cube-id}(T^\ell), \text{type}(T^\ell), 0, \dots, 0)_{2^d}. \quad (3.14)$$

This resembles the Morton index of the associated cube Q_T of T , since we can write this as

$$\tilde{m}(Q_T) = (\text{cube-id}(Q^1), \dots, \text{cube-id}(Q^\ell), 0, \dots, 0)_{2^d}. \quad (3.15)$$

3.5. Properties of the TM-index. In this section we show that the TM-index has similar properties than the Morton index for cubes. We are particularly interested in locality properties stating that refining a simplex only locally changes the order given by the TM-index. We begin with stating the uniqueness of the TM-index if additionally a level ℓ is given.

Proposition 13. *Together with a refinement level ℓ , the TM-index $m(T)$ uniquely determines a d -simplex in \mathcal{T}_d .*

Proof. If $\ell = 0$ then there is only one simplex of level ℓ in \mathcal{T}_d , which is T_d^0 . So let $\ell > 0$ and $m = m(T)$ be given as in (3.11) and let ℓ be the level of T . From m we can compute the x, y (and z) coordinates of the associated cube of T . We can also compute the type of T from the TM-index. By Lemma 6 this information uniquely determines T . \square

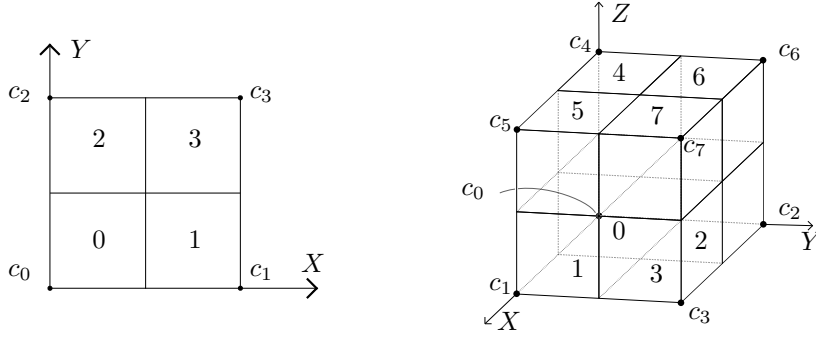


FIGURE 3.2. Left: A square is refined to four children, each of which corresponds to a corner of the square. The number of the corner is the cube-id of that child. Right: In three dimensions a cube is refined to eight children. Their cube-ids and corner numbers are shown as well.

For the Morton index \tilde{m} for cubes the following important properties are known [46]:

- The Morton indices of the descendants of a parent cube are larger or equal to the index of the parent cube.
- A Morton index of a cube Q is the prefix of an index of a cube P of higher level than Q if and only if P is a descendant of Q .
- Refining only changes the SFC locally. Thus, if Q is a cube and P is a cube with $\tilde{m}(Q) < \tilde{m}(P)$ and P is not a descendant of Q , then $\tilde{m}(Q') < \tilde{m}(P)$ for each descendant Q' of Q .

We show below that these properties also hold for d -simplices and the TM-index described by (3.11).

Theorem 14. For arbitrary d -simplices $T \neq S \in \mathcal{T}_d$ the TM-index satisfies:

- If S is a descendant of T then $m(T) \leq m(S)$.
- If $\ell_T < \ell_S$, then $m(T)$ is a prefix of $m(S)$ if and only if S is a descendant of T .
- If $m(T) < m(S)$ and S is no descendant of T , then for each descendant T' of T we have

$$m(T) \leq m(T') < m(S). \quad (3.16)$$

The proof of Theorem 14 requires some work and we need to show a technical result first. Hereby, we consider only the case $d = 3$, since for $d = 2$ the argument is completely analogous. The technical result will be that the set of all TM-indices is a subset of the Morton indices for 6-dimensional cubes. Since the properties (i)-(iii) hold for these cubes it will then follow that they hold for tetrahedra as well. To this end, for a given tetrahedron $T \in \mathcal{T}_3$ we interpret each entry b_j of $B(T)$ as a 3-digit binary number

$$b_j = (b_j^2 b_j^1 b_j^0)_2, \quad (3.17)$$

which is possible since $b_j \in \{0, \dots, 5\}$. We obtain three new \mathcal{L} -tuples B^2, B^1, B^0 satisfying

$$B = B^2 \dot{\perp} B^1 \dot{\perp} B^0 \quad (3.18)$$

and thus we can rewrite the TM-index as

$$m(T) = Z \dot{\perp} Y \dot{\perp} X \dot{\perp} B^2 \dot{\perp} B^1 \dot{\perp} B^0. \quad (3.19)$$

Note that we can interpret each B^i as an \mathcal{L} -digit binary number for which we have $0 \leq B^i < 2^\mathcal{L}$. Let now \mathcal{Q} denote the set of all 6-dimensional cubes that are a child of the cube $Q_0 := [0, 2^\mathcal{L}]^6$:

$$\mathcal{Q} = \{Q \mid Q \text{ is a descendant of } Q_0 \text{ of level } 0 \leq \ell \leq \mathcal{L}\}. \quad (3.20)$$

Since a cube $Q \in \mathcal{Q}$ is uniquely determined by the six coordinates (x_0, \dots, x_5) of its anchor node plus its level ℓ , we will also write $Q = Q_{(x_0, \dots, x_5), \ell}$. Note that the Morton index for a cube can be defined as the bitwise interleaving of its anchor node coordinates [28]:

$$\tilde{m}(Q) = X^5 \dot{\downarrow} X^4 \dot{\downarrow} X^3 \dot{\downarrow} X^2 \dot{\downarrow} X^1 \dot{\downarrow} X^0. \quad (3.21)$$

Proposition 15. *The map*

$$\begin{aligned} \Phi: \mathcal{T}_3 &\longrightarrow \mathcal{Q}, \\ T &\longmapsto Q_{(B^0(T), B^1(T), B^2(T), x(T), y(T), z(T)), \ell(T))} \end{aligned} \quad (3.22)$$

is injective and satisfies

$$\tilde{m}(\Phi(T)) = m(T). \quad (3.23)$$

Furthermore, it fulfills the property that T' is a child of T if and only if $\Phi(T')$ is a child of $\Phi(T)$.

Proof. The equation $m(T) = \tilde{m}(\Phi(T))$ follows directly from the definitions of the TM-indices on \mathcal{T}_3 and \mathcal{Q} . From Lemma 13 we conclude that Φ is injective. Let now $T', T \in \mathcal{T}_3$, where T' is a child of T . Let furthermore $\ell = \ell(T)$. We know that $Q' := \Phi(T')$ is a child of $Q := \Phi(T)$ if and only if for each $i \in \{0, \dots, 5\}$ it holds

$$x_i(Q') \in \left\{ x_i(Q), x_i(Q) + 2^{\mathcal{L} - (\ell + 1)} \right\}. \quad (3.24)$$

Because of the underlying cube structure (compare figure 2.3) we know that the x coordinate of the anchor node of T' satisfies

$$x(T') \in \left\{ x(T), x(T) + 2^{\mathcal{L} - (\ell + 1)} \right\} \quad (3.25)$$

and likewise for $Y(T')$ and $Z(T')$. Therefore, (3.24) holds for $i = 3, 4, 5$. By definition $B^j(T')$ is the same as $B^j(T)$ except at position $\mathcal{L} - (\ell + 1)$, where

$$B^j(T')_{\mathcal{L} - (\ell + 1)} = b_{\mathcal{L} - (\ell + 1)}^j(T') \in \{0, 1\}, \quad (3.26)$$

and

$$B^j(T)_{\mathcal{L} - (\ell + 1)} = 0. \quad (3.27)$$

Hence, we conclude that (3.24) also holds for $i = 0, 1, 2$. So $\Phi(T')$ is a child of $\Phi(T)$.

To show the other implication, let us assume that $\Phi(T')$ is a child of $\Phi(T)$. Since $\ell(T') = \ell(\Phi(T')) > 0$, T' has a parent and we denote it by P . In the argument above we have shown that $\Phi(P)$ is the parent of $\Phi(T')$ and because each cube has a unique parent the identity $\Phi(P) = \Phi(T)$ must hold. Therefore, we get $P = T$ since Φ is injective; thus, T' is the child of T . \square

Inductively we conclude that T' is a descendant of T if and only if $\Phi(T')$ is a descendant of $\Phi(T)$. Now Theorem 14 follows, because the desired properties (i)-(iii) hold for the Morton index of cubes. \square

Part (iii) from Theorem 14 tells us that the descendants of a simplex T are traversed before any other simplices with a higher TM-index than T are traversed. However, the order that the children of T have relative to each other can be different to the order of children of another simplex T' . In particular the order of the simplices defined by the TM-index differs from the order (2.2) defined by Bey. We observe this behavior in two dimensions in Figure 3.1 on the right-hand side: For the level 1 triangles of type 0 the children are traversed in the order

$$T_0, T_1, T_3, T_2 \quad (3.28)$$

and the children of the level 1 triangle of type 1 are traversed in the order

$$T_0, T_3, T_1, T_2. \quad (3.29)$$

In fact, the order of the children of a simplex T only depends on the type of T as we show in the following Proposition.

Proposition 16. *If $T, T' \in \mathcal{T}_d$ are two d -simplices with $\text{type}(T) = \text{type}(T')$, then there exists a permutation σ of $\{0, \dots, 2^d - 1\}$ such that*

$$\begin{aligned} m(T_{\sigma(0)}) &< m(T_{\sigma(1)}) < \dots < m(T_{\sigma(2^d-1)}), \\ &\text{and} \\ m(T'_{\sigma(0)}) &< m(T'_{\sigma(1)}) < \dots < m(T'_{\sigma(2^d-1)}). \end{aligned} \quad (3.30)$$

Thus, the children of T and the children of T' are in the same order with respect to their TM-index.

Proof. Certainly, we obtain σ and σ' with

$$\begin{aligned} m(T_{\sigma(0)}) &< m(T_{\sigma(1)}) < \dots < m(T_{\sigma(2^d-1)}), \\ m(T'_{\sigma'(0)}) &< m(T'_{\sigma'(1)}) < \dots < m(T'_{\sigma'(2^d-1)}). \end{aligned} \quad (3.31)$$

It remains to show that $\sigma' = \sigma$. Let $\ell = \ell(T)$ and $\ell' = \ell(T')$. Since the TM-indices of the children of T do all agree up to level ℓ , we see, using the notation from (3.12), that their order σ depends only on the $d+1$ numbers (z is omitted for $d=2$)

$$z_{\mathcal{L}-(\ell+1)}(T_i), \quad y_{\mathcal{L}-(\ell+1)}(T_i), \quad x_{\mathcal{L}-(\ell+1)}(T_i) \quad \text{and} \quad b_{\mathcal{L}-(\ell+1)}(T_i). \quad (3.32)$$

The same argument applies to σ' and ℓ' . From now on we carry out the computations for $d=3$. Since $\text{type}(T) = \text{type}(T')$ we can write

$$T = \lambda T' + \vec{c}, \quad (3.33)$$

with

$$\lambda = 2^{\ell' - \ell}, \quad \vec{c} = \begin{pmatrix} x(T) - x(T') \\ y(T) - y(T') \\ z(T) - z(T') \end{pmatrix}. \quad (3.34)$$

Since the refinement rules (2.2) commute with scaling and translation we also obtain

$$T_i = \lambda T'_i + \vec{c} \quad (3.35)$$

for the children of T and T' and therefore

$$(3.36)$$

for $0 \leq i < 2^d$. Furthermore, we have

$$x_{\mathcal{L}-(\ell+1)}(T_i) = (x(T_i) - x(T))2^{-\mathcal{L}+(\ell+1)} \quad (3.37)$$

from which we derive

$$\begin{aligned} x_{\mathcal{L}-(\ell+1)}(T_i) &= \lambda(x(T'_i) - x(T'))2^{-\mathcal{L}+(\ell+1)} \\ &= 2^{\ell'-\ell}(x(T'_i) - x(T'))2^{-\mathcal{L}+(\ell+1)} \\ &= (x(T'_i) - x(T'))2^{-\mathcal{L}+(\ell'+1)} \\ &= x_{\mathcal{L}-(\ell'+1)}(T'_i), \end{aligned} \quad (3.38)$$

and analogously

$$\begin{aligned} y_{\mathcal{L}-(\ell+1)}(T_i) &= y_{\mathcal{L}-(\ell'+1)}(T'_i), \\ z_{\mathcal{L}-(\ell+1)}(T_i) &= z_{\mathcal{L}-(\ell'+1)}(T'_i). \end{aligned} \quad (3.39)$$

This shows that the tetrahedral Morton order of the children of T and T' are the same and σ' must equal σ . \square

4. The space-filling curve associated to the TM-index. By interpreting the TM-indices as d -ary numbers as in (3.12) we introduce a total order on the set of all possible TM-indices. Therefore, it gives rise to a SFC for any refinement \mathcal{S} of T_d^0 . Space-filling curves play an important role in partitioning a given refinement among a set of processors. In this section we further examine the SFC from the TM-index. We begin with giving a recursive description of it, which is similar to the descriptions of the Sierpinski curve and other cubical SFC [21]. We then continue with proving an upper bound on the number of corner-connected and face-connected components of any partition obtained from the SFC.

4.1. Recursive Definition of the SFC. Proposition 16 tells us that for each type b we get a permutation σ_b of $\{0, \dots, 2^d - 1\}$ such that for any d -simplex T of type b we have

$$m(T_{\sigma_b(0)}) < m(T_{\sigma_b(1)}) < \dots < m(T_{\sigma_b(2^d-1)}) \quad (4.1)$$

for the children of T . Thus, if we consider the order of the children of T the child T_i is at position $\sigma_b(i)$.

Definition 17. Let $T \in \mathcal{T}_d$ such that T' 's parent P has type b and T is the i -th child of P according to Bey's order (2.2), $0 \leq i < 2^d$. We call the number $\sigma_b(i)$ the *local index* of the d -simplex T and use the notation

$$I_{\text{loc}}(T) := \sigma_b(i). \quad (4.2)$$

By definition, the local index of the root simplex is zero, $I_{\text{loc}}(T_d^0) := 0$. Table 4.1 lists the local indices for each parent type.

I_{loc}	Child				I_{loc}	Child											
	2D	T_0	T_1	T_2		T_3	T_4	T_5	T_6	T_7							
b	0	0	1	3	2	b	0	0	1	4	7	2	3	6	5		
	1	0	2	3	1		1	0	1	5	7	2	3	6	4		
2	0	3	4	7	1		2	0	3	4	7	1	2	6	5		
3	0	1	6	7	2		3	4	0	1	6	7	2	3	4	5	
4	0	3	5	7	1		2	4	6	0	3	5	7	1	2	4	6
5	0	3	6	7	2		1	4	5	0	3	6	7	2	1	4	5

TABLE 4.1

The local index of a d -simplex T . For each type b , the 2^d children T_0, \dots, T_{2^d-1} of a simplex of type b can be ordered according to their TM-indices. The position of the i -th child according to this order is the local index $I_{\text{loc}}(T_i)$.

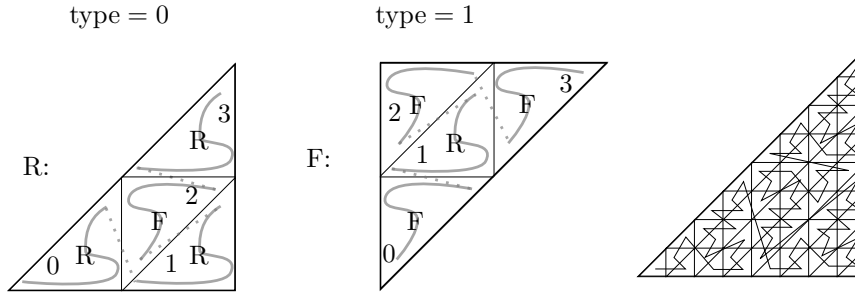


FIGURE 4.1. Left: Using the notation from [21] we recursively describe the space-filling curve arising from the TM-index for triangles. The numbers inside the children triangles are their local index. Writing R for the refinement scheme for type 0 triangles and F for type 1 triangles. This pattern can be obtained from Tables 3.1 and 4.1. Right: The Space-filling curve for a uniform level 3 refinement of the root triangle.

Thus, we know for each type $0 \leq b < d!$ how the children of a tetrahedron of type b are traversed. This gives us an approach for describing the SFC arising from the TM-index in a recursive fashion [21]. By specifying for each possible type b the order and types of the children of a type b simplex, we can build up the SFC. In Figure 4.1 we describe the SFC for triangles in this way. In three dimensions it is not convenient to draw the six pictures for the different types, but the SFC can be derived similarly from Tables 3.1 and 4.1.

4.2. The number of connected components of the SFC. When load-balancing a refinement of T_d^0 according to the space-filling curve, each process is assigned a portion of the mesh that is covered by a section of the space-filling curve. Where two of the resulting subdomains belonging to different processes share corners or faces these processes usually have to communicate with each other. Since inter-process communication is a relatively slow operation we desire that the boundary area of a subdomain is small. The area of a subdomain's boundary relative to its interior rises with the number of connected components of the subdomain. We show that the number of components that are at least corner-connected is at most two. In the next section we also prove a level-dependent upper bound on the number of face-connected components.

Our proof is divided in several lemmas and follows roughly [4] and [13], where it

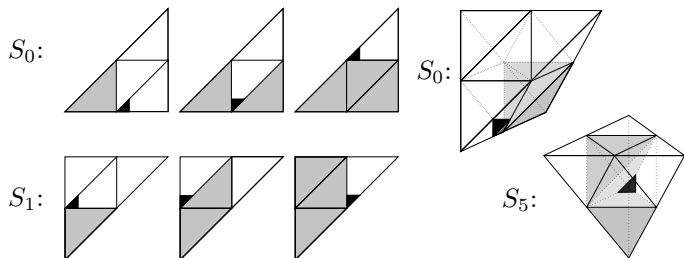


FIGURE 4.2. The illustrated proof of Lemma 18. If a type b simplex is refined uniformly to level ℓ , then any segment of the space-filling curve, consisting of $j > 0$ full level 1 subsimplices (the grey regions) starting at the first one and one additional level ℓ subsimplex (shown in black), is connected. We show all cases in 2D and two of the 42 cases in 3D (types 0 and 5).

is shown that the number of face-connected components for an arbitrary section of the Morton curve on a hypercube is at most two.

Lemma 18. *If a d -simplex of any type b is uniformly refined to level ℓ then any segment of the space-filling curve starting in the first or ending in the last level ℓ subsimplex has exactly one connected component.*

Proof. We only give the argument for the case that the section is beginning at the first simplex. The other case is analogous and will also follow as a special case of Lemma 20. We proceed by induction over ℓ and the case $\ell = 0$ is obvious, since there is only one simplex in the refinement. So let $\ell > 0$ and let j be the local index of the level 1 subsimplex in which the last segment of the curve lies. If $j = 0$ the curve lies completely inside a level 1 subsimplex and the claim follows by induction. If not we have j level 1 subsimplices that are fully contained in the section of the curve plus one incomplete one. By induction we have one connected component in this last incomplete level 1 subsimplex. Let t denote the first simplex of this subsimplex, it remains to show that t is connected to the segment of the first j full level 1 subsimplices. This can be easily done by an enumeration of all cases as is shown in Figure 4.2. \square

Lemma 19. *Any contiguous section of level 1 subsimplices of T_d^0 has one connected component.*

Proof. It suffices to check this for segments of length two, since, if any longer segment would have two or more connected components, we can construct a segment of length two with two connected components by taking the last simplex in the first component of the long segment and the first simplex in the second component. There are only three segments of length two in dimension $d = 2$ and seven in dimension $d = 3$ for which the claim can easily be checked by enumeration. \square

Lemma 20. *Let a segment of the space-filling curve for a uniform level- ℓ refinement of T_d^0 consist of one full level 1 subsimplex plus one single level ℓ simplex at the end, then this segment has one connected component.*

Proof. By Lemma 18 the full level 1 segment is connected and it remains to show that the additional level ℓ simplex is connected to one of the simplices in this segment. We denote this level ℓ simplex by t , the full level 1 simplex by T and let j be the local index of T . If t and T lie in the same level 1 subcube of T_d^0 then t and the first level ℓ simplex in T both have the origin of this cube as their anchor node and are therefore

connected. The remaining cases are $j \in \{0, 3, 6\}$ (6 only in 3D). In each of these cases one vertex of T is the same as the origin of the level 1 subcube that t lies in, which is its anchor node. We conclude that also in these cases t is connected to at least one level ℓ simplex in T . \square

Proposition 21. *Any contiguous segment of the space-filling curve of a uniform level ℓ refinement of T_d^0 has at most two connected components.*

Proof. If the segment is contained in a level $\ell-1$ subsimplex, we are done by induction. Otherwise, we can divide the segment into three pieces: At the beginning the segment is one (possibly incomplete) level 1 subsimplex that ends at its last level ℓ subsimplex, then there is one contiguous segment of zero to $2^d - 2$ full level-1 subsimplices, and at the end is one (possibly incomplete) level 1 subsimplex that starts at its first level ℓ subsimplex. From Lemma 18 it follows that the first and the third piece are each connected. The second piece is connected by Lemma 19. We apply Lemma 20 to show that the second and the third piece form in fact one connected component, leading to at most two connected components in total. \square

Theorem 22. *Let \mathcal{S} be a refinement (not necessarily uniform) of T_d^0 , then any contiguous segment of the space-filling curve on \mathcal{S} has at most two connected components.*

Proof. By the same argument as in [13], let ℓ be the highest level occurring in \mathcal{S} . Since refining a simplex in the segment of the space-filling curve and adding all its children to the segment does not change the number of connected components, we simply refine each simplex in \mathcal{S} to level ℓ and apply Proposition 21. \square

4.3. The number of face-connected components. In this subsection we examine the number of face-connected components of a segment of the space-filling curve. As we show in Figure 4.3 there exist cases where the number of face-connected components in a uniform 2d level ℓ refinement can be as high as $2(\ell - 1)$. We show that this estimate is in fact sharp. We also show that in three dimensions the number of face-connected components does not exceed $2\ell + 1$. There exists an example with 2ℓ face-connected components and we conjecture that 2ℓ is in fact the sharp estimate. The proof of these bounds is fairly analogous to the proof of Theorem 22 and again we separate the proof into several lemmas.

Lemma 23. *Let a segment of the space-filling curve for a uniform level ℓ refinement of T_d^0 consist of several full level 1 subsimplices plus one single level ℓ simplex at the end or at the beginning, then this segment has at most two face-connected components.*

Lemma 24. *If a d -simplex of type i is uniformly refined to level ℓ then any segment of the space-filling curve ending in the last simplex or starting in the first has at most $\ell + 1$ face-connected components. For $d = 2$ a segment ending in the last simplex of a type 0 refinement simplex has just one face-connected component, as well as a segment starting in the first simplex of a type 1 refinement.*

Proof. The proof for the last statement is identical to the proof of Lemma 18. We give now the argument for a segment starting in the first simplex, since the other case is analogous. The case $\ell = 1$ can be obtained from the proof of Lemma 20. For the case $\ell > 1$ we separate the segment into subsegments according to the levels of full subsimplices, namely:

- At the beginning, 0 to 2^d full level 1 subsimplices.

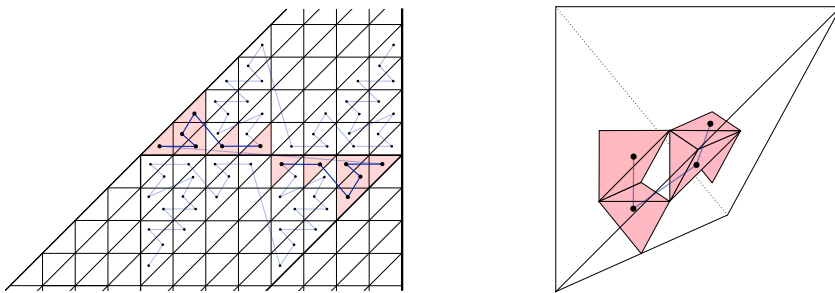


FIGURE 4.3. Left: A segment of the 2d space-filling curve on a level 4 refinement of T_2^0 with six face-connected components (shaded). Only the significant parts of the space-filling curve are shown. The construction is recursive and can be applied to every level ℓ showing that the number of face-connected components in 2d can be as high as $2(\ell - 1)$. We prove that this estimate is sharp. Right: A 3d level 2 refinement of T_3^0 with four ($= 2\ell$) face-connected components. We show that the number of face-connected components is bounded by $2\ell + 1$.

- After that, 0 to $2^d - 1$ full level 2 subsimplices.
- ⋮
- Finally at the end, 0 to $2^d - 1$ full level ℓ subsimplices.

Because of the $\ell = 1$ case, each of these segments has at most two face-connected components and, according to Lemma 23, if one segment has two components, then the next one is connected to it. Thus, from each of these ℓ segments we get at most one additional face-connected component, plus possibly two for the last segment. This leads to at most $\ell + 1$ face-connected components in total. \square

Proposition 25. *In 2d, any contiguous segment of the space-filling curve of a uniform level $\ell \geq 2$ refinement of T_2^0 has at most $2(\ell - 1)$ face-connected components. For $\ell = 1$ there are at most two face-connected components. In 3d the number of face-connected components is bounded by $2\ell + 1$, for each $\ell \geq 0$.*

Proof. We first show that for both dimensions the number of face-connected components is bounded by $2\ell + 1$. If the given segment is contained in a level $\ell - 1$ subsimplex we are done by induction. Otherwise we can divide the segment into three (possibly empty) pieces: At the beginning the segment is one incomplete level 1 subsimplex, that ends at its last level ℓ subsimplex; then there is one contiguous segment of full level 1 subsimplices and at the end the segment is one (possibly incomplete) level 1 subsimplex that starts at its first level ℓ subsimplex. From Lemma 24 follows that the first and the last piece have at most ℓ face-connected components each. By Lemma 23 the second piece has at most two face-connected components and if it does, then it is face-connected to the first and to the third piece. Thus, it adds only one face-connected component to the total number. We end up with

$$\ell + 1 + \ell = 2\ell + 1 \tag{4.3}$$

face-connected components.

Let now $\ell \geq 2$ and $d = 2$. We conclude from Lemma 24 that the case that the first and last subsegment add ℓ face-connected components can only occur if the first segment is contained in the only level 1 subtriangle of type 1 (local index 2). Then, the last segment must be contained in the last level 1 subtriangle of type 0 (local index 3). It follows that the middle segment must be empty, therefore adding no face-connected

component. Furthermore the first and the last subsegment can not be contained only in the last respectively first level 2 subtriangle of their level 1 subtriangle, because then they would only have at most $\ell - 1$ face-connected components. Now the last level ℓ triangle in the second last level 2 subtriangle of the first subsegment is face-connected to the first level 2 subtriangle in the last subsegment (for a visualization see Figure 4.3). The same holds for the second level 2 subtriangle in the last subsegment. Therefore, we can further subtract two face-connected components from the estimate, leading to at most

$$\ell + \ell - 2 = 2(\ell - 1) \tag{4.4}$$

face-connected components in 2d. \square

Theorem 26. *Let \mathcal{S} be a 2d refinement (not necessarily uniform) of T_2^0 with maximum refinement level ℓ , then any contiguous segment of the space-filling curve on \mathcal{S} has at most $2(\ell - 1)$ face-connected components. In 3d the number of face-connected components is at most $2\ell + 1$.*

An example of a segment with 2ℓ face-connected components is given by the segment of SFC-indices 22–25 of a uniform level 2 refinement of T_3^0 . We illustrate this in Figure 4.3. We believe that the case that the first and the last piece described in the proof of Proposition 25 have ℓ face-connected components each and that additionally the middle piece adds one component does not occur.

Conjecture 27. *In 3d, the number of face-connected components is bounded by 2ℓ and this estimate is sharp.*

5. Algorithms on simplices. In this section we present fundamental algorithms that operate on d -simplices in \mathcal{T}_d . These algorithms include computations of parent and child simplices, computation of face-neighbors and computations involved with the TM-index. To simplify the notation we will carry out all algorithms for tetrahedra and then describe how to modify them for triangles. We introduce the data type **Tet** and will not distinguish between the abstract concept of a **Tet** and the geometric object (tetrahedron or triangle) that it represents. A **Tet** T has the following entries:

- $T.\ell$ — the refinement level of T ,
- $T.\vec{x} = (T.x, T.y, T.z)$ — The x, y and z coordinates of T 's anchor node, also sometimes referred to as $T.x_0, T.x_1$, and $T.x_2$,
- $T.b$ — The type of T .

In two-dimensional computations the parameter $T.z$ is not present. To avoid confusion we use the notation \vec{x} to denote vectors in \mathbb{Z}^d and x (without arrow) for integers, thus numbers in \mathbb{Z} . From Lemma 6 we know that the entries stored in a **Tet** suffice to uniquely identify a d -simplex $T \in \mathcal{T}$. Most algorithms we present here only need this data as input resulting in a fixed storage size per **Tet**. If, for example, the maximum level \mathcal{L} is 32 or less, then the coordinates can be stored in a 4-byte integer each and the level and type occupy one byte each, for a total storage of $3 * 4 + 1 + 1 = 14$ bytes per **Tet** in 3D and $2 * 4 + 1 + 1 = 10$ bytes in 2D. Most of the algorithms that we present here run in constant time independent of the maximum level \mathcal{L} . The only algorithms running in constant time but depending on the level \mathcal{L} or $T.\ell$, thus having $\mathcal{O}(\mathcal{L})$ runtime, will be the ones for computing the consecutive index from a **Tet** and the one for initializing a **Tet** according to a given consecutive index. Hence, we will show how to replace repetitive calls of these relatively involved algorithms by more efficient ones.

5.1. The coordinates of a d -simplex. The coordinates of the $d + 1$ nodes of a d -simplex T can be obtained easily from its Tet-id, the relation (2.3) and simple arithmetic: If T is a d -simplex of level ℓ , type b and anchor node $\vec{x}_0 \in \mathbb{Z}^d$, then

$$T = 2^{\mathcal{L}-\ell} S_b + \vec{x}_0. \quad (5.1)$$

Hence, in order to compute the coordinates of T we can take the coordinates of S_b , as given in (2.3), and then use relation (5.1). A closer look at (2.3) reveals that it is not necessary to examine all coordinates of S_b in order to compute the x_i , but that they can also be computed arithmetically. This computation is carried out in Algorithm 5.1.

Algorithm 5.1: Coordinates(Tet T)

```

1  $X \leftarrow (T.\vec{x}, 0, 0, 0)$ 
2  $h \leftarrow 2^{\mathcal{L}-\ell}$ 
3  $i \leftarrow \lfloor \frac{T.b}{2} \rfloor$  /* Replace with  $i \leftarrow T.b$  for 2D */
4 if  $T.b \% 2 = 0$  then
5   |  $j \leftarrow (i + 2) \% 3$ 
6 else
7   |  $j \leftarrow (i + 1) \% 3$ 
8  $X[1] \leftarrow X[0] + he_i$ 
9  $X[2] \leftarrow X[1] + he_j$  /* Replace with  $X[2] \leftarrow X[0] + (h, h)^t$  for 2D */
10  $X[3] \leftarrow X[0] + (h, h, h)^t$  /* Remove this line for 2D */
11 return  $X$ 
```

5.2. Parent and child. In this section we describe how to compute the Tet-ids of the parent $P(T)$ and of the 2^d children $T_i, 0 \leq i < 2^d$ of a given d -simplex $T \in \mathcal{T}_d$. Computing the anchor node coordinates of the parent is easy, since their first $T.\ell - 1$ bits correspond to the coordinates of T 's anchor node and the rest of their bits is zero. For computing the type of $P(T)$, we will need the function

$$\begin{aligned} \text{Pt: } \{0, \dots, 2^d - 1\} \times \{0, \dots, d! - 1\} &\longrightarrow \{0, \dots, d! - 1\} \\ (\text{cube-id}(T), T.b) &\longmapsto P.b, \end{aligned} \quad (5.2)$$

giving the type of T 's parent in dependence of its cube-id and type. In Figure 5.1 we list all values of this function for $d \in \{2, 3\}$.

Algorithm 5.2: c-id(Tet T , int ℓ) *The cube-id of T^ℓ .*

```

1  $i \leftarrow 0, h \leftarrow 2^{\mathcal{L}-\ell}$ 
2  $i \mid = (T.x \& h) ? 1 : 0$ 
3  $i \mid = (T.y \& h) ? 2 : 0$ 
4  $i \mid = (T.z \& h) ? 4 : 0$  /* Remove this line for 2D */
5 return  $i$ 
```

The algorithm **Parent** to compute the parent of T now puts these two ideas together, computing the coordinates and type of $P(T)$. Algorithm 5.3 shows an implementation. It uses Algorithm 5.2 to compute the cube-id of a d -simplex.

For the computation of one child T_i of T for a given $i \in \{0, \dots, 2^d - 1\}$ we look at the definition of the subsimplices in (2.2) and see that in order to compute the anchor node of the child we need to know some of the node coordinates x_0, \dots, x_d

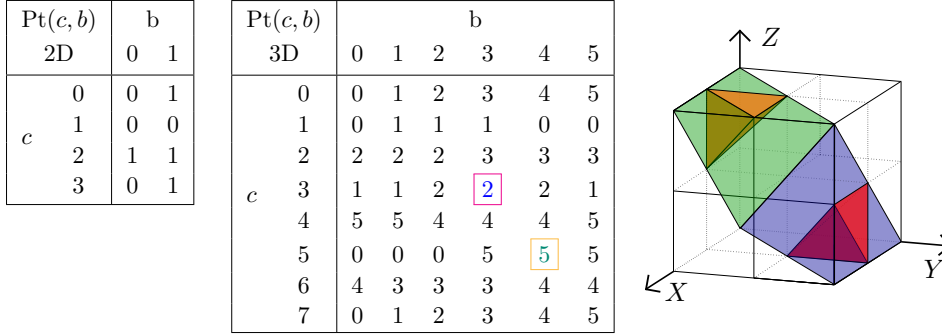


FIGURE 5.1. The type of the parent of a d -simplex T can be determined from T 's cube-id c and type b . Left: The values of Pt from (5.2) in the 2D case. Middle: The values of the function Pt in the 3D case. Right: Two examples showing the computation in 3D. (1) The small tetrahedron in the top left corner (orange) has cube-id 5 and type 4, its parent (green) can be seen to have type 5. (2) The small tetrahedron at the bottom right (red) has cube-id 3 and type 3, its parent (blue) has type 2.

Algorithm 5.3: Parent(Tet T)

```

1  $h \leftarrow 2^{\mathcal{L}-T.\ell}$ 
2  $P.\ell \leftarrow T.\ell - 1$ 
3  $P.x \leftarrow T.x \ \& \ \neg h$ 
4  $P.y \leftarrow T.y \ \& \ \neg h$ 
5  $P.z \leftarrow T.z \ \& \ \neg h$ 
6  $P.b \leftarrow Pt(c-id(T, T.\ell), T.b)$ 
7 return  $P$ 

```

/* Remove this line for 2D */
/* See (5.2) and Figure 5.1 for Pt */

of the parent simplex T . These can be obtained via Algorithm 5.1. However, it is more efficient to only compute those coordinates of T that are actually necessary. To compute the Tet-id of T_i we will also need to know its type. The type of T_i depends only on the type of T , as can be seen in Table 3.1. Algorithm 5.4 shows now how to compute the coordinates of the i -th child of T in Bey's order.

When we would like to compute the i -th child of a d -simplex T of type b with respect to the tetrahedral Morton order — thus the child T_k of T with $I_{loc}(T_k) = i$ — we just call Algorithm 5.4 with $\sigma_b^{-1}(i)$ as input. The permutations σ_b^{-1} are available from Table 4.1.

Algorithm 5.4: Child(Tet T , int i)

```

1  $X \leftarrow Coordinates(T)$ 
2 if  $i = 0$  then  $j \leftarrow 0$ 
3 else if  $i \in \{1, 4, 5\}$  then  $j \leftarrow 1$ 
4 else if  $i \in \{2, 6, 7\}$  then  $j \leftarrow 2$ 
5 else if  $i = 3$  then  $j \leftarrow 3$ 
6  $T_i.\vec{x} \leftarrow \frac{1}{2}(X[0] + X[j])$ 
7  $T_i.b \leftarrow Ct(T.b, i)$ 

```

/* If $i = 3$ then $j \leftarrow 1$ for 2D */
/* See Table 3.1 */

5.3. Neighbor simplices. Many applications, for example finite element methods, need to gather information about the face-neighboring simplices of a given simplex in a refinement. In this section we describe a level-independent constant-runtime algorithm to compute the Tet-id of the neighbor along a specific face f of

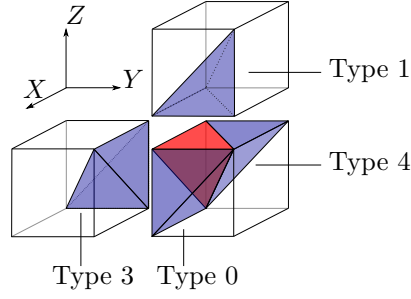


FIGURE 5.2. A tetrahedron T of type 5 (in the middle, red) and its four face neighbors (blue) of types 1, 0, 4 and 3, drawn with their associated cubes (exploded view). We see that the type of T 's neighbors depends only on its type, while their node coordinates relative to T 's depend additionally on T 's level.

a given d -simplex T . This algorithm is very lightweight since it only requires a few arithmetic computations involving the Tet-id of T and the number f . In comparison to other approaches [10, 26] to find neighbors in constant time, our algorithm does not involve the computation of any of T 's ancestors.

The $d + 1$ faces of a d -simplex $T = [x_0, \dots, x_d]$ are numbered f_0, \dots, f_d in such a way that face f_i is the face not containing the node x_i . To examine the situation where two d -simplices of the same level share a common face, let \mathcal{T}_d^ℓ denote a uniform refinement of T_d^0 of a given level $0 \leq \ell \leq \mathcal{L}$,

$$\mathcal{T}_d^\ell := \{ T \mid T \text{ is a descendant of } T_d^0 \text{ of level } \ell \} \subset \mathcal{T}^d. \quad (5.3)$$

\mathcal{T}_d can be seen as the disjoint union of all the \mathcal{T}_d^ℓ :

$$\mathcal{T}_d = \bigcup_{\ell=0}^{\mathcal{L}} \mathcal{T}_d^\ell. \quad (5.4)$$

Given a d -simplex $T \in \mathcal{T}_d^\ell$ and a face number $i \in \{0, \dots, d\}$, denote T 's neighbor in \mathcal{T}_d^ℓ across face $f = f_i$ by $\mathcal{N}_f(T)$. The face number of the neighbor simplex $\mathcal{N}_f(T)$ across which T is its neighbor will be denoted by $\tilde{f}(T)$. Hence, the relation

$$\mathcal{N}_{\tilde{f}(T)}(\mathcal{N}_f(T)) = T \quad (5.5)$$

holds for each face f of T .

Our aim is to compute the Tet-id of $\mathcal{N}_f(T)$ and $\tilde{f}(T)$ from the Tet-id of T . Using the underlying cube structure this problem can be solved for each occurring type of d -simplex separately, and the solution scheme is independent of the coordinates of T and of ℓ . In Figure 5.2 the situation for a tetrahedron of type 5 is illustrated, and in Tables 5.1 and 5.2 we present the general solution for each type.

Using these tables, a constant time computation of the Tet-id of $\mathcal{N}_f(T)$ and of $\tilde{f}(T)$ from the Tet-id of T is possible and the three dimensional is carried out in Algorithm 5.5. Note that this algorithm uses arithmetic expressions in $T.b$ to avoid the sixfold distinction of cases. Of course it is possible that $\mathcal{N}_f(T)$ does not belong to \mathcal{T}_d^ℓ any longer. If this is the case then f was part of the boundary of the root simplex T_d^0 . We describe in the next section how we can decide in constant time whether $\mathcal{N}_f(T)$ is in T^ℓ or not.

2D	f	0	1	2
$T.b = 0$	$\mathcal{N}_{\tilde{f}.b}$	1	1	1
	$\mathcal{N}_{\tilde{f}.x}$	$T.x + h$	$T.x$	$T.x$
	$\mathcal{N}_{\tilde{f}.y}$	$T.y$	$T.y$	$T.y - h$
	\tilde{f}	2	1	0
$T.b = 1$	$\mathcal{N}_{\tilde{f}.b}$	0	0	0
	$\mathcal{N}_{\tilde{f}.x}$	$T.x$	$T.x$	$T.x - h$
	$\mathcal{N}_{\tilde{f}.y}$	$T.y + h$	$T.y$	$T.y$
	\tilde{f}	2	1	0

TABLE 5.1

The table of face neighbors in 2D. For each possible type $b \in \{0, 1\}$ of a triangle T and each of its faces $f = f_i, i \in \{0, 1, 2\}$, the type, anchor node coordinates and corresponding face number \tilde{f} of T 's neighbor across f are shown. In the 2D case we can directly compute $\mathcal{N}.b = 1 - T.b$ and $\tilde{f} = 2 - f$. Here, $h = 2^{\mathcal{L}-\ell}$ refers to the length of one square of level ℓ .

3D	f	0	1	2	3	3D	f	0	1	2	3
$T.b = 0$	$\mathcal{N}_{\tilde{f}.b}$	4	5	1	2	$T.b = 3$	$\mathcal{N}_{\tilde{f}.b}$	5	4	2	1
	$\mathcal{N}_{\tilde{f}.x}$	$T.x + h$	$T.x$	$T.x$	$T.x$		$\mathcal{N}_{\tilde{f}.x}$	$T.x$	$T.x$	$T.x$	$T.x - h$
	$\mathcal{N}_{\tilde{f}.y}$	$T.y$	$T.y$	$T.y$	$T.y - h$		$\mathcal{N}_{\tilde{f}.y}$	$T.y + h$	$T.y$	$T.y$	$T.y$
	$\mathcal{N}_{\tilde{f}.z}$	$T.z$	$T.z$	$T.z$	$T.z$		$\mathcal{N}_{\tilde{f}.z}$	$T.z$	$T.z$	$T.z$	$T.z$
	\tilde{f}	3	1	2	0		\tilde{f}	3	1	2	0
$T.b = 1$	$\mathcal{N}_{\tilde{f}.b}$	3	2	0	5	$T.b = 4$	$\mathcal{N}_{\tilde{f}.b}$	2	3	5	0
	$\mathcal{N}_{\tilde{f}.x}$	$T.x + h$	$T.x$	$T.x$	$T.x$		$\mathcal{N}_{\tilde{f}.x}$	$T.x$	$T.x$	$T.x$	$T.x - h$
	$\mathcal{N}_{\tilde{f}.y}$	$T.y$	$T.y$	$T.y$	$T.y$		$\mathcal{N}_{\tilde{f}.y}$	$T.y$	$T.y$	$T.y$	$T.y$
	$\mathcal{N}_{\tilde{f}.z}$	$T.z$	$T.z$	$T.z$	$T.z - h$		$\mathcal{N}_{\tilde{f}.z}$	$T.z + h$	$T.z$	$T.z$	$T.z$
	\tilde{f}	3	1	2	0		\tilde{f}	3	1	2	0
$T.b = 2$	$\mathcal{N}_{\tilde{f}.b}$	0	1	3	4	$T.b = 5$	$\mathcal{N}_{\tilde{f}.b}$	1	0	4	3
	$\mathcal{N}_{\tilde{f}.x}$	$T.x$	$T.x$	$T.x$	$T.x$		$\mathcal{N}_{\tilde{f}.x}$	$T.x$	$T.x$	$T.x$	$T.x$
	$\mathcal{N}_{\tilde{f}.y}$	$T.y + h$	$T.y$	$T.y$	$T.y$		$\mathcal{N}_{\tilde{f}.y}$	$T.y$	$T.y$	$T.y$	$T.y - h$
	$\mathcal{N}_{\tilde{f}.z}$	$T.z$	$T.z$	$T.z$	$T.z - h$		$\mathcal{N}_{\tilde{f}.z}$	$T.z + h$	$T.z$	$T.z$	$T.z$
	\tilde{f}	3	1	2	0		\tilde{f}	3	1	2	0

TABLE 5.2

The table of face neighbors in 3D. For each possible type $b \in \{0, 1, 2, 3, 4, 5\}$ of a tetrahedron T and each of its faces $f = f_i, i \in \{0, 1, 2, 3\}$ the type $\mathcal{N}_f(T).b$ of T 's neighbor across f , its coordinates of the anchor node $\mathcal{N}_f(T).x, \mathcal{N}_f(T).y, \mathcal{N}_f(T).z$ and the corresponding face number $\tilde{f}(T)$, across which T is $\mathcal{N}_f(T)$'s neighbor, are shown.

For completeness, we summarize the geometry and numbers of d -simplices touching each other via a corner ($d = 2$ or $d = 3$) or edge (only $d = 3$). In this paper we do not list these neighboring tetrahedra in detail.

For $d = 3$ each corner in the mesh \mathcal{T}_3^ℓ has 24 adjacent tetrahedra (See Figure 5.3), thus each tetrahedron has at each corner 23 other tetrahedra that share this particular corner. For $d = 2$ the situation is similar with six triangles meeting at each corner. To examine the number of adjacent tetrahedra to an edge we distinguish three types of edges in \mathcal{T}_d^ℓ as displayed in Figure 5.4:

1. edges that are also edges in the underlying hexahedral mesh,
2. edges that are the diagonal of a side of a cube in the hexahedral mesh,
3. edges that correspond to the inner diagonal of a cube in the hexahedral mesh.

Edges of the first and the third kind have six adjacent tetrahedra each and edges of

Algorithm 5.5: Face-neighbor(Tet T , int f)

```

1  $b \leftarrow T.b, x_0 \leftarrow T.x_0, x_1 \leftarrow T.x_1, x_2 \leftarrow T.x_2$ 
2 if  $f = 1$  or  $f = 2$  then
3    $\tilde{f} \leftarrow f$  if  $(b \% 2 = 0$  and  $f = 2)$  or  $(b \% 2 \neq 0$  and  $f = 1)$  then
4      $b \leftarrow b + 1$ 
5   else
6      $b \leftarrow b - 1$ 
7 else
8    $\tilde{f} \leftarrow 3 - f$ 
9    $h \leftarrow 2^{\mathcal{L} - T.\ell}$ 
10  if  $f = 0$  then /*  $f = 0$  */
11     $i \leftarrow b \text{ div } 2$ 
12     $x_i \leftarrow T.x_i + h$ 
13     $b \leftarrow b + (b \% 2 = 1 ? 2 : 4)$ 
14  else /*  $f = 3$  */
15     $i \leftarrow (b + 3) \% 6 \text{ div } 2$ 
16     $x_i \leftarrow T.x_i - h$ 
17     $b \leftarrow b + (b \% 2 = 0 ? 2 : 4)$ 
18 return  $(x_0, x_1, x_2, b \% 6, \tilde{f})$ 

```

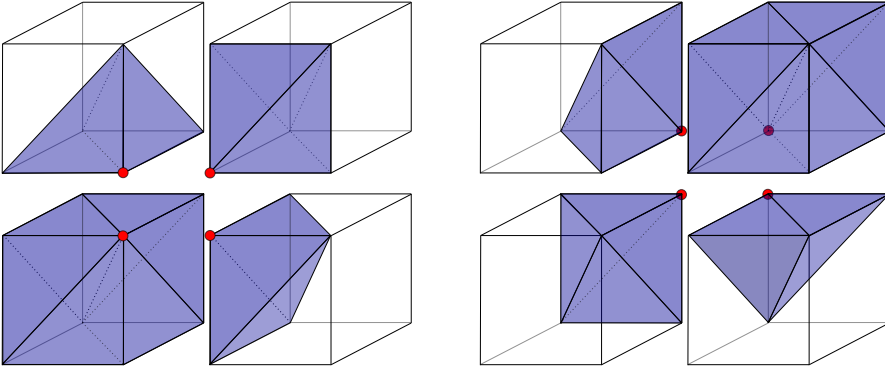


FIGURE 5.3. A corner in the mesh \mathcal{T}_3^ℓ (marked with a red dot) and its adjacent tetrahedra (blue). All shown red dots mark the same corner and are actually identified. We observe that the corner has 24 adjacent tetrahedra and 8 adjacent cubes, where two diagonally opposite cubes contribute 6 tetrahedra each and the other cubes contribute 2 tetrahedra each. From symmetry reasons, this configuration is the same for each corner in the mesh.

the second kind do have four adjacent tetrahedra each, see Figure 5.4.

5.4. The exterior of the root simplex. When computing neighboring d -simplices it is possible that the neighbor in question does not belong to the root simplex T_d^0 but lies outside of it. If we look at face neighbors of a d -simplex T , the fact that the considered neighbor lies outside means that the respective face was on the boundary of T_d^0 . In order to check whether a computed d -simplex is outside the base simplex, we investigate a more general problem: Given anchor node coordinates $(x_0, y_0)^t \in \mathbb{Z}^2$, resp. $(x_0, y_0, z_0)^t \in \mathbb{Z}^3$, a type b and a level ℓ , decide whether the corresponding d -simplex N lies inside or outside of the root tetrahedron T_d^0 : $N \in \mathcal{T}_d^\ell$ or $N \notin \mathcal{T}_d^\ell$. At the end of this section we furthermore generalize this to the problem of deciding for any two d -simplices N and T whether N lies outside of T or not. We

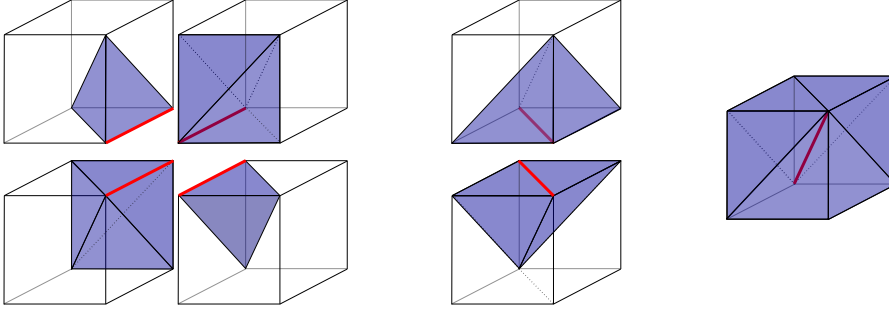


FIGURE 5.4. When we consider tetrahedra adjacent to edges in the mesh \mathcal{T}_3^ℓ we distinguish three cases. Left: These edges that are also edges of the underlying hexahedral mesh. Adjacent to these edges are six tetrahedra. Middle: These edges that are the diagonal of a side of a cube in the underlying hexahedral mesh. These edges have four tetrahedra adjacent to them. Right: This edge is the diagonals of a cube in the underlying hexahedral mesh. As in the first case these edges have six tetrahedra adjacent to them.

solve this problem in constant time and independent of the levels of N and T .

Let us now examine the three dimensional case. Looking at T_3^0 we see that two of its boundary faces correspond to faces of the root cube, namely the intersections of T_3^0 with the $y = 0$ and the $x = 2^{\mathcal{L}}$ planes. The other two boundary faces of T_3^0 are the intersections with the $x = z$ and the $y = z$ planes. Thus, the boundary of T_3^0 can be described as the intersection of T_3^0 with those planes. We will refer to the latter two planes as E_1 and E_2 .

Let now N be a tetrahedron with anchor node $(x_0, y_0, z_0)^t \in \mathbb{Z}^3$ of type b and level ℓ . Let furthermore $(x_i, y_i, z_i)^t$ be the coordinates of node i of N , since we know that $(x_i, y_i, z_i)^t \geq (x_0, y_0, z_0)^t$ (component wise) we directly conclude that if $x_0 \geq 2^{\mathcal{L}}$ or $y_0 < 0$ then $N \notin \mathcal{T}_3$. Because the outer normal vectors of T_3^0 on the two faces intersecting with E_1 and E_2 are

$$\vec{n}_1 = \frac{1}{\sqrt{2}} \begin{pmatrix} -1 \\ 0 \\ 1 \end{pmatrix} \quad \text{and} \quad \vec{n}_2 = \frac{1}{\sqrt{2}} \begin{pmatrix} 0 \\ 1 \\ -1 \end{pmatrix}, \quad (5.6)$$

we also conclude that $N \notin \mathcal{T}_3$ if $z_0 - x_0 > 0$ or $y_0 - z_0 > 0$. Now we have already covered all the cases except those where the anchor node of N lies directly in E_1 or E_2 . In these cases we cannot solve the problem by looking at the coordinates of the anchor node alone, since there exist tetrahedra $T' \in \mathcal{T}_3$ with anchor nodes lying in one of these planes (see Figure 5.5 for an illustration of the analogous case in 2D). This depends on the type of the tetrahedron in question. We observe that a tetrahedron $T' \in \mathcal{T}_3$ with anchor node lying in E_1 can have the types 0, 1 or 2 and a tetrahedron with anchor node lying in E_2 can have the types 0, 4 or 5. We conclude that to check whether N is outside of the root tetrahedron we have to check if any one of six conditions is fulfilled. In fact these conditions fit into the general form below with $x_i = x$, $x_j = y$, $x_k = z$ and T as the root tetrahedron, thus $T.x = T.y = T.z = 0$ and $T.b = 0$.

These generalized conditions solve the problem to check for any two given tetrahedra N and T , whether N lies outside of T or not.

Proposition 28. *Given two d -simplices N, T with $N.\ell \geq T.\ell$, then N is outside of*

2D	$T.b$		3D	$T.b$					
	0	1		0	1	2	3	4	5
x_i	x	y	x_i	x	x	y	y	z	z
x_j	y	x	x_j	y	z	z	x	x	y
			x_k	z	y	x	z	y	x

TABLE 5.3

Following the general scheme described in this section to compute whether a given d -simplex N lies outside of another given d -simplex T , we give the coordinates x_i, x_j and x_k in dependence of the type of T .

the simplex T — which is equivalent to saying that N is no descendant of T — if and only if at least one of the following conditions is fulfilled.

For $d = 2$:

$$N.x_i - T.x_i \geq 2^{T.\ell}, \quad (5.7a)$$

$$N.x_j - T.x_j < 0, \quad (5.7b)$$

$$(N.x_j - T.x_j) - (N.x_i - T.x_i) > 0, \quad (5.7c)$$

$$N.x_i - T.x_i = N.x_j - T.x_j \text{ and } N.b = \begin{cases} 1 & \text{if } T.b = 0, \\ 0 & \text{if } T.b = 1. \end{cases} \quad (5.7d)$$

And for $d = 3$:

$$N.x_i - T.x_i \geq 2^{T.\ell}, \quad (5.8a)$$

$$N.x_j - T.x_j < 0, \quad (5.8b)$$

$$(N.x_k - T.x_k) - (N.x_i - T.x_i) > 0, \quad (5.8c)$$

$$(N.x_j - T.x_j) - (N.x_k - T.x_k) > 0, \quad (5.8d)$$

$$N.x_k - T.x_k = N.x_i - T.x_i$$

$$\text{and } N.b \in \begin{cases} \{T.b + 1, T.b + 2, T.b + 3\}, & \text{if } T.b \text{ is even,} \\ \{T.b - 1, T.b - 2, T.b - 3\}, & \text{if } T.b \text{ is odd,} \end{cases} \quad (5.8e)$$

$$N.x_j - T.x_j = N.x_k - T.x_k$$

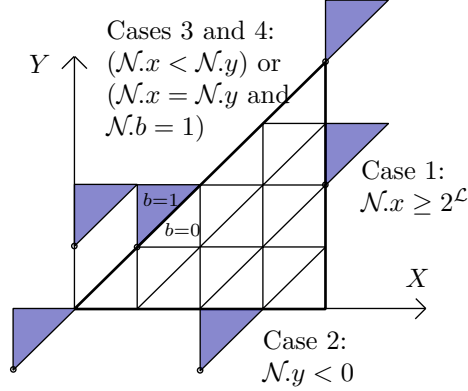
$$\text{and } N.b \in \begin{cases} \{T.b - 1, T.b - 2, T.b - 3\}, & \text{if } T.b \text{ is even,} \\ \{T.b + 1, T.b + 2, T.b + 3\}, & \text{if } T.b \text{ is odd.} \end{cases} \quad (5.8f)$$

The coordinates x_i, x_j and x_k are chosen in dependence of the type of T according to Table 5.3.

Proof. By shifting N by $(-T.\vec{x})$ we reduce the problem to checking whether the shifted d -simplex lies outside of a d -simplex with anchor node $\vec{0}$ and level $T.\ell$ and type $T.b$. For $d = 3$ the proof is analogous to the above argument, where we considered the case $b = 0$ and $\ell = 0$. In two dimensions the situation is even simpler, since there exists only one face of the root triangle that is not a coordinate axis (see Figure 5.5). \square

5.5. A consecutive index. In contrast to the Morton index for cubes, the TM-index for d -simplices does not produce a consecutive range of numbers. Therefore, two simplices T and T' of level ℓ that are direct successors/predecessors with respect to the tetrahedral Morton order do not necessarily fulfill $m(T) = m(T') \pm 2^{d(\mathcal{L}-\ell)}$ or $m(T) = m(T') \pm 1$. For $d = 3$ this follows directly from the fact that each b^j

FIGURE 5.5. A uniform level 2 refinement of the triangle T^0 in 2D and triangles lying outside of it with their anchor nodes marked. When deciding whether a triangle with given anchor node coordinates lies outside of T^0 there are four cases to consider, one for each face of T^0 . For the two faces lying parallel to the X - respectively Y -axis it suffices to check whether the x -coordinate is greater than or equal to $2^{\mathcal{L}}$, or whether the y -coordinate is smaller than 0. Similarly one can conclude that the triangle lies outside of T^0 if its x -coordinate is smaller than its y -coordinate. If both coordinates agree (and none of the previous cases applies) then the given triangle is outside T^0 if and only if its type is 1.



occupies three bits but there are only six values that each b^j can assume, since there are only six different types. In two dimensions this follows from the fact that not every combination of anchor node coordinates and type can occur for triangles in \mathcal{T}_2 , the triangle with anchor node $(0, 0)$ and type 1 being one example. This also means that the largest occurring TM-index is bigger than $2^{d\mathcal{L}} - 1$.

However, it is possible to construct a consecutive index that respects the order given by the TM-index. We show here how to compute it. Since in practice it is more convenient to work with this consecutive index instead of the TM-index, our aim is to construct for each level ℓ a consecutive index $I(T) \in \{0, \dots, 2^{d\ell} - 1\}$, such that

$$\forall T, S \in \mathcal{T}_d^\ell: \quad I(T) < I(S) \Leftrightarrow m(T) < m(S). \quad (5.9)$$

This index can also be understood as a bijection

$$I: \{m \in \mathbb{N}_0 \mid m = m(T) \text{ for a } T \in \mathcal{T}_d^\ell\} \xrightarrow{\cong} \{0, \dots, 2^{d\ell} - 1\}, \quad (5.10)$$

mapping the TM-indices of level ℓ d -simplices to a consecutive range of numbers. It is obvious that $I(T_d^0) = 0$. The index $I(T)$ can be easily computed as the ℓ -digit 2^d -ary number consisting of the local indices as digits, thus

$$I(T) = (I_{\text{loc}}(T^1), \dots, I_{\text{loc}}(T^\ell))_{2^d}. \quad (5.11)$$

Algorithm 5.6 shows an implementation of this computation. It can be done directly from the Tet-id of T , thus it is not necessary to compute the TM-index of T first.

Algorithm 5.6: $I(\text{Tet } T)$

```

1  $I \leftarrow 0, b \leftarrow T.b$ 
2 for  $T.\ell \geq i \geq 1$  do
3    $c \leftarrow \text{c-id}(T, i)$ 
4    $I \leftarrow I + I_{\text{loc}}^b(c) * 8^i$ 
5    $b \leftarrow \text{Pt}(c, b)$ 
6 return  $I$ 

```

/* See Table 5.4; multiply with 4^i for 2D */

The inverse operation of computing T from $I(T)$ and a given level ℓ can be carried out in a similar fashion; see Algorithm 5.7. For each $0 \leq i \leq \ell$ we look up the type

b and the cube-id of T^i from $I_{\text{loc}}(T^i)$ and the type of $\text{Parent}(T^i) = T^{i-1}$ (starting with $\text{type}(T^0) = 0$) via Tables 5.5 and 5.6. From the cube-id's we can build up the anchor node coordinates of T . The last computed type is the type of T .

Algorithm 5.7: T(consecutive index I , int ℓ)

```

1  $T.x, T.y, T.z \leftarrow 0, b \leftarrow 0$ 
2 for  $1 \leq i \leq \ell$  do
3   Get  $I_{\text{loc}}(T^i)$  from  $I$  /* See (5.11) */
4    $c \leftarrow c\text{-id}(T^i), b \leftarrow T^i.b$  /* See Tables 5.5 and 5.6 */
5   if  $c \& 1$  then  $T.x \leftarrow T.x + 2^{\mathcal{L}-i}$ 
6   if  $c \& 2$  then  $T.y \leftarrow T.y + 2^{\mathcal{L}-i}$ 
7   if  $c \& 4$  then  $T.z \leftarrow T.z + 2^{\mathcal{L}-i}$  /* Remove this line for 2D */
8  $T.b \leftarrow b$ 
9 return  $T$ 

```

5.6. Successor and predecessor. Calculating the TM-index corresponding to a particular consecutive index is relatively expensive, since it involves a loop over all refinement levels, thus some 10 to 30 in extreme cases. We are often in the situation to compute a whole range of d -simplices. This occurs for example when creating an initial uniform refinement of a given mesh (See Algorithm **New** in Section 6.1). The task is, for a given consecutive index I , a level ℓ and a count n to find the n level- ℓ simplices following the d -simplex corresponding to the consecutive index I , that is, the d -simplices corresponding to the n consecutive indices $I, I+1, \dots, I+n-1$. Ideally, this operation should run linearly in n , independent of ℓ , but if we used Algorithm 5.7 to create each of the $n+1$ simplices we would have a runtime of $\mathcal{O}(n\mathcal{L})$. In order to achieve the desired linear runtime we introduce the operations **Successor** and **Predecessor** that run in average $\mathcal{O}(1)$ time. These operations compute from a given d -simplex T of level ℓ with consecutive index I_T the d -simplex T' whose consecutive index is $I_T + 1$, respectively $I_T - 1$. Thus, T' is the next level ℓ simplex in the SFC after T (resp. the previous one). Algorithm 5.8 that we introduce to solve this problem does not require knowledge about the consecutive indices I_T and $I_T \pm 1$ and can be computed significantly faster than Algorithm 5.7; see Lemma 29.

Algorithm 5.8: Successor(Tet T)

```

1 return Successor_recursion( $T, T, T, \ell$ )

Function Successor_recursion(Tet  $T$ , Tet  $T'$ , int  $\ell$ )
1  $c \leftarrow c\text{-id}(T, \ell)$ 
2 From  $c$  and  $b$  look up  $i := I_{\text{loc}}(T^\ell)$  /* See Table 5.4 */
3  $i \leftarrow (i+1) \% 8$ 
4 if  $i = 0$  then /* Enter recursion (in rare cases) */
5    $T' \leftarrow \text{Successor\_recursion}(T, T', \ell - 1)$ 
6    $\hat{b} \leftarrow T'.b$  /*  $\hat{b}$  stores the type of  $T'^{\ell-1}$  */
7 else
8    $\hat{b} \leftarrow \text{Pt}(c, b)$ 
9 From  $\hat{b}$  and  $I_{\text{loc}} = i$  look up  $(c', b')$  /* See Tables 5.5 and 5.6 */
10 Set the level  $\ell$  entries of  $T'.x, T'.y$  and  $T'.z$  to  $c'$ 
11  $T'.b \leftarrow b'$ 
12 return  $T'$ 

```

To compute the predecessor of T we only need to reverse the sign in Line 3 in the

$I_{loc}^b(c)$	cube-id c				$I_{loc}^b(c)$	cube-id c									
2D	0	1	2	3	3D	0	1	2	3	4	5	6	7		
b	0	0	1	1	3	b	0	0	1	1	4	1	4	4	7
	1	0	2	2	3		1	0	1	2	5	2	5	4	7
							2	0	2	3	4	1	6	5	7
							3	0	3	1	5	2	4	6	7
							4	0	2	2	6	3	5	5	7
							5	0	3	3	6	3	6	6	7

TABLE 5.4

The local index of a tetrahedron $T \in \mathcal{T}$ in dependence of its cube-id c and type b .

cube-id(T)	$I_{loc}(T)$				cube-id(T)	$I_{loc}(T)$									
2D	0	1	2	3	3D	0	1	2	3	4	5	6	7		
$P.b$	0	0	1	1	3	$P.b$	0	0	1	1	5	5	5	7	
	1	0	2	2	3		1	0	1	1	1	3	3	3	7
							2	0	2	2	2	3	3	3	7
							3	0	2	2	2	6	6	6	7
							4	0	4	4	4	6	6	6	7
							5	0	4	4	4	5	5	5	7

TABLE 5.5

For a tetrahedron $T \in \mathcal{T}$ of local Index I_{loc} whose parent P has type $P.b$ we give the cube-id of T .

Successor_recursion subroutine of Algorithm 5.8.

Lemma 29. Algorithm 5.8 has constant average runtime (independent of \mathcal{L}).

Proof. Because each operation in the algorithm can be executed in constant time, the average runtime is nc , where c is a constant (independent of \mathcal{L}) and $n - 1$ is the number of average recursion steps. Since in consecutive calls to the algorithm the variable i will cycle through 0 to $2^d - 1$ we conclude that the recursion is on average executed in every 2^d -th step, allowing for a geometric series argument. \square

We see in Algorithm 5.8 the usefulness of the consecutive index. Because we are using this index instead of the TM-index, computing the index of the successor/predecessor only requires adding/subtracting 1 to the given index. Opposed to this, computing the TM-index of a successor/predecessor would involve more subtle computations.

6. High-level AMR algorithms. To develop the complete AMR functionality required by numerical applications, we aim at a forest of quad-/octrees in the spirit of [14, 23]. Key top-level algorithms are:

- **New.** Generate an initial mesh structure from a given triangulation.
- **Adapt.** Adapt (refine and coarsen) a mesh according to a given criterion.
- **Partition.** Partition a mesh among all processors such that the load is balanced, possibly according to weights.
- **Balance.** Establish a 2:1 size condition between neighbors in a given refined mesh:. The levels of any two neighboring simplices must differ by at most 1.

$T.b$		$I_{loc}(T)$				$T.b$		$I_{loc}(T)$							
2D		0	1	2	3	3D		0	1	2	3	4	5	6	7
$P.b$	0	0	0	1	0	$P.b$	0	0	0	4	5	0	1	2	0
	1	1	0	1	1		1	1	2	3	0	1	5	1	
					2		2	0	1	2	2	3	4	2	
					3		3	3	4	5	1	2	3	3	
					4		4	2	3	4	0	4	5	4	
					5		5	0	1	5	3	4	5	5	

TABLE 5.6

For a tetrahedron $T \in \mathcal{T}$ of local Index I_{loc} whose parent P has type $P.b$ we give the type of T .

- **Ghost.** For each process, assemble the layer of directly neighboring elements owned by other processes.
- **Iterate.** Iterate through the local mesh, executing a callback function on each element and on all inter-element interfaces.

Since partitioning via SFC only uses the SFC index as information, we refer to already existing descriptions of **Partition** for hexahedral or simplicial space-filling curves [14,34]. **Balance**, **Ghost** and **Iterate** are sophisticated parallel algorithms and require additional theoretical work, which is beyond the scope of this paper.

Here, we briefly describe **New** and **Adapt**. In the forest-of-trees approach we model an adaptive mesh by a coarse mesh of level 0 d -simplices, the *trees*. Each level 0 simplex is identified with the root simplex T_d^0 and then refined adaptively to produce the fine mesh of d -simplices. These simplices are partitioned among all processors, thus each processor has a range of trees that it owns, where the first and last one are possibly incomplete. An entity \mathcal{F} of the structure **forest** consists of the following entries

- $\mathcal{F}.C$ — the coarse mesh,
- $\mathcal{F}.K$ — The processor-local trees.
- $\mathcal{F}.E_k$ — For each local tree k the list of processor-local simplices in tetrahedral Morton order.

We acknowledge that **New** and **Adapt** are essentially communication-free, but still serve well to exercise some of the fundamental algorithms described earlier.

6.1. New. The **New** algorithm creates a partitioned uniform level ℓ refined forest from a given coarse mesh. To achieve this, we first compute the first and last d -simplex belonging to the current processor p . From this range we can calculate which trees belong to p and for each of these trees the consecutive index of the first and last d -simplex on this tree. We then create the first simplex in a tree by a call to **T** (Algorithm 5.7) and create the rest by successive calls to the **Successor** algorithm (Algorithm 5.8). Our **New** algorithm is very similar to the **New** algorithm presented in [14] for hexahedral cells in Z -order. The difference is the call to **Successor** instead of **T**, which we do to avoid the $\mathcal{O}(\ell)$ runtime of **T** in the case of simplices. Our numerical tests, displayed in Figure 7.1, show that the runtime of **New** is in fact linear in the number of elements and does not depend on the level ℓ .

6.2. Adapt. The **Adapt** algorithm creates a new forest by refining and coarsening the d -simplices of a given forest according to a callback function. It does this by traversing the d -simplices of each tree in tetrahedral Morton order and passing

Algorithm 6.1: `New`(Coarse Mesh C , int ℓ)

```

1  $n \leftarrow 2^{d\ell}$ ,  $N \leftarrow nK$ ; /*  $d$ -simplices per tree and global number of  $d$ -simplices */
2  $g_{\text{first}} \leftarrow \lfloor Np/P \rfloor$ ,  $g_{\text{last}} \leftarrow \lfloor N(p+1)/P \rfloor - 1$ ; /* Global numbers of first and last.. */
3  $k_{\text{first}} \leftarrow \lfloor g_{\text{first}}/n \rfloor$ ,  $k_{\text{last}} \leftarrow \lfloor g_{\text{last}}/n \rfloor$ ; /* ..local simplex and local tree range */
4 for  $t \in \{k_{\text{first}}, \dots, k_{\text{last}}\}$  do
5    $e_{\text{first}} \leftarrow (t = k_{\text{first}}) ? g_{\text{first}} - nt : 0$ ;
6    $e_{\text{last}} \leftarrow (t = k_{\text{last}}) ? g_{\text{last}} - nt : n - 1$ ;
7    $T \leftarrow \mathcal{T}(e_{\text{first}}, \ell)$ ; /* Call Algorithm 5.7 */
8    $\mathcal{E}_k \leftarrow \{T\}$ ;
9   for  $e \in \{e_{\text{first}}, \dots, e_{\text{last}} - 1\}$  do
10     $T \leftarrow \text{Successor}(T)$ ;
11     $\mathcal{E}_k \leftarrow \mathcal{E}_k \cup \{T\}$ 

```

them to the callback function. If the current d -simplex and its $2^d - 1$ successors form a family (all have the same parent) then the whole family is passed to the callback. This callback function accepts either one or 2^d d -simplices as input plus the index of the current tree. In both cases, a return value greater than zero means that the first input d -simplex should be refined, thus its 2^d children are added in tetrahedral Morton order to the new forest. Additionally, if the input consists of 2^d simplices, they form a family and a return value smaller than zero means that this family should be coarsened, thus replaced by their parent. If the callback function returns zero, the first given d -simplex remains unchanged and is added to the new forest and `Adapt` continues with the next d -simplex in the current tree. The `Adapt` algorithm creates a new forest from the given one and can handle recursive refinement/coarsening. For the recursive part we make use of the following reasonable assumptions:

- A d -simplex that was created in a refine step will not be coarsened during the same adapt call.
- A d -simplex that was created in a coarsening step will not be refined during the same adapt call.

From these assumptions we conclude that for recursive refinement we only have to consider those d -simplices that were created in a previous refinement step and that we only have to care about recursive coarsening directly after we processed a d -simplex that was not refined and could be the last d -simplex in a family. If refinement and coarsening are not done recursively, the runtime of `Adapt` is linear in the number of d -simplices of the given forest.

7. Performance evaluation. We present scaling and runtime tests¹ for `New` and `Adapt` on the JUQUEEN supercomputer at Forschungszentrum Juelich [16], an IBM BlueGene/Q system with 28,672 nodes consisting of 16 IBM PowerPC A2 @ 1.6 GHz and 16 GB Ram per node. We also present one runtime study on the full MIRA system at the Argonne Leadership Computing facility, which has the same architecture as JUQUEEN and 49,152 nodes. The biggest occurring number of mesh cells is around 8.5×10^{11} tetrahedra with 13 million elements per process.

The first two tests are a strong scaling (up to 131k processes) and a runtime study of `New` in 3D – shown in Figure 7.1. For both these tests we use a coarse mesh of 512 tetrahedra. We time the `New` algorithm with input level 8 (resp. level 10 for higher numbers of processes) We do the runtime study to examine whether `New` has

¹Version v0.1 available at <https://bitbucket.org/cburstedde/t8code.git>

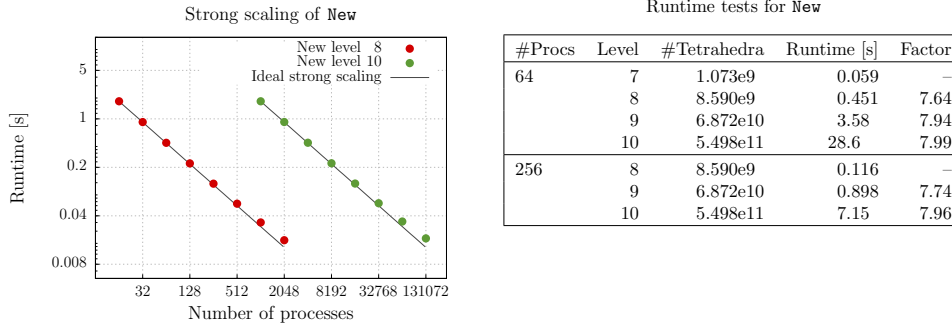


FIGURE 7.1. Runtime tests for *New* on *JUQUEEN*. Left: Two strong scaling studies. A new uniform level 8 (red) and level 10 (green) refinement of a coarse mesh of 512 root tetrahedra, carried out with 16 up to 2048 processes and 1024 up to 131072 processes with 16 processes per compute node. Right: The data shows that the runtime of *New* is linear in the number of generated elements and does not additionally depend on the level. The uniform refinement is created from a coarse mesh of 512 root tetrahedra. For the first computation on 64 processes we use 1 process per compute node and for the computation on 256 processes we use 2 processes per node.

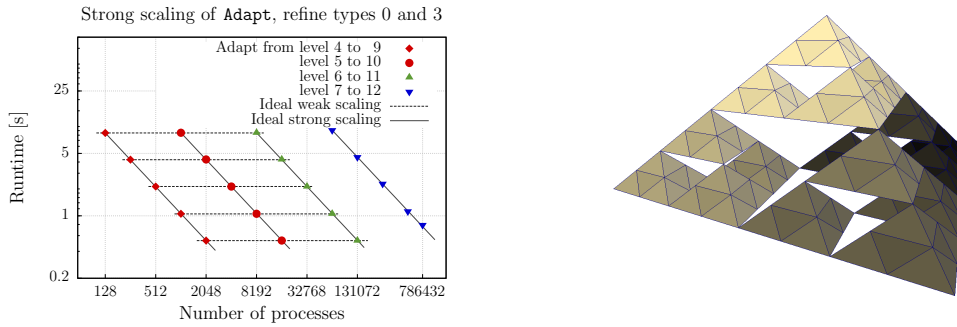


FIGURE 7.2. Strong scaling for *Adapt* with a fractal refinement pattern. Starting from an initial level k on a coarse mesh of 512 tetrahedra we refine recursively to a maximal final level $k + 5$. The refinement callback is such that only subtetrahedra of types 0 and 3 are refined. Left: Strong and weak scaling on *JUQUEEN* with up to 131,072 processes and strong scaling on *MIRA* with up to 786,432 processes. On both systems we use 16 processes per compute node. The level 12 mesh consists of 858,588,635,136 tetrahedra. Right: An initial level 0 and final level 3 refinement according to the fractal pattern. The subtetrahedra of levels 1 and 2 are transparent.

the proposed level-independent linear runtime in the number of generated tetrahedra, which can be read from the results presented in the Table in Figure 7.1.

The last test is *Adapt* with a recursive non-uniform refinement pattern. The starting point for all runs is a mesh obtained by uniformly refining a coarse mesh of 512 tetrahedra to a given initial level k . This mesh is then refined recursively using a single *Adapt* call, where only the tetrahedra of types 0 and 3 whose level does not exceed the fine level $k + 5$ are refined recursively. The resulting mesh on each tetrahedron resembles a fractal pattern similar to the Sierpinski tetrahedron. We do several strong and weak scaling runs on *JUQUEEN* starting with 128 processes and scaling up to 131,072. The setting is 16 processes per compute node. We finally do another strong scaling run on the full system of the *MIRA* supercomputer at the Argonne Leadership Computing Facility with 786,432 processes and again 16 processes per compute node. Figure 7.2 shows our runtime results.

8. Conclusion. We present a new encoding for adaptive non-conforming triangular and tetrahedral mesh refinement based on Bey’s red refinement rule. We identify six different types of tetrahedra (and two types of triangles) and prescribe an ordering of the children for each of these types that differs from Bey’s original order. By introducing an embedding of the mesh elements into a Cartesian coordinate structure, we define a tetrahedral Morton index that can be computed using bitwise interleaving similar to the Morton index for cubes. This tetrahedral Morton index shares some properties with the well-known cubical one and allows for a memory efficient random access storage of the mesh elements.

Exploiting the Cartesian coordinate structure, we develop several level independent constant time algorithms on simplices. These include finding parent, children and face-neighbors of a given mesh element as well as computing the next and previous element according to the space-filling curve.

To verify that partitions generated using the new SFC are not arbitrarily disconnected we prove that any section of the SFC has at most two connected components and at most $2(\ell + 1)$ face-connected components, where ℓ is the biggest occurring refinement level.

Encouraged by the present results, we will continue to implement a full suite of AMR algorithms based on this scheme and to examine its performance in practice.

Acknowledgements. The authors gratefully acknowledge support by the Bonn Hausdorff Centre for Mathematics (HCM) funded by the Deutsche Forschungsgemeinschaft (DFG). H. acknowledges additional support by the Bonn International Graduate School for Mathematics (BIGS) as part of HCM. We would also like to thank Tobin Isaac for his thoughts on software interfacing.

The authors would like to thank the Gauss Centre for Supercomputing (GCS) for providing computing time through the John von Neumann Institute for Computing (NIC) on the GCS share of the supercomputer JUQUEEN [16] at Jülich Supercomputing Centre (JSC). GCS is the alliance of the three national supercomputing centres HLRS (Universität Stuttgart), JSC (Forschungszentrum Jülich), and LRZ (Bayerische Akademie der Wissenschaften), funded by the German Federal Ministry of Education and Research (BMBF) and the German State Ministries for Research of Baden-Württemberg (MWK), Bayern (StMWFK) and Nordrhein-Westfalen (MIWF). This research used resources of the Argonne Leadership Computing Facility, which is a DOE Office of Science User Facility supported under Contract DE-AC02-06CH11357.

REFERENCES

- [1] Volkan Akçelik, Jacobo Bielak, George Biros, Ioannis Epanomeritakis, Antonio Fernandez, Omar Ghattas, Eui J. Kim, Julio Lopez, David R. O’Hallaron, Tiankai Tu, and John Urbanic. High resolution forward and inverse earthquake modeling on terascale computers. In *SC03: Proceedings of the International Conference for High Performance Computing, Networking, Storage, and Analysis*. ACM/IEEE, 2003. Gordon Bell Prize for Special Achievement.
- [2] Frédéric Alauzet and Adrien Loseille. On the use of space filling curves for parallel anisotropic mesh adaptation. In Brett W. Clark, editor, *Proceedings of the 18th International Meshing Roundtable*, pages 337–357. Springer Berlin Heidelberg, 2009.
- [3] I. Babuska and W. C. Rheinboldt. Error estimates for adaptive finite element computations. *SIAM Journal on Numerical Analysis*, 15(4):pp. 736–754, 1978.
- [4] Michael Bader. *Space-Filling Curves: An Introduction with Applications in Scientific Computing*. Texts in Computational Science and Engineering. Springer, 2012.
- [5] Wolfgang Bangerth, Carsten Burstedde, Timo Heister, and Martin Kronbichler. Algorithms

- and data structures for massively parallel generic adaptive finite element codes. *ACM Transactions on Mathematical Software*, 38(2):14:1–14:28, 2011.
- [6] Wolfgang Bangerth, Ralf Hartmann, and Guido Kanschat. deal.II – a general-purpose object-oriented finite element library. *ACM Transactions on Mathematical Software*, 33(4):24, 2007.
- [7] Eberhard Bänsch. Local mesh refinement in 2 and 3 dimensions. *IMPACT of Computing in Science and Engineering*, 3(3):181 – 191, 1991.
- [8] Jürgen Bey. Der BPX-Vorkonditionierer in drei Dimensionen: Gitterverfeinerung, Parallelisierung und Simulation. *Universität Heidelberg*, 1992. Preprint.
- [9] Jürgen Bey. Simplicial grid refinement: on Freudenthal’s algorithm and the optimal number of congruence classes. *Numerische Mathematik*, 85(1):1–29, 2000.
- [10] Kolja Brix, Ralf Massjung, and Alexander Voss. Refinement and connectivity algorithms for adaptive discontinuous Galerkin methods. *SIAM Journal on Scientific Computing*, 33(1):66–101, 2011.
- [11] Thang Nguyen Bui and Curt Jones. Finding good approximate vertex and edge partitions is NP-hard. *Information Processing Letters*, 42(3):153 – 159, 1992.
- [12] Carsten Burstedde, Omar Ghattas, Michael Gurnis, Tobin Isaac, Georg Stadler, Tim Warburton, and Lucas C. Wilcox. Extreme-scale AMR. In *SC10: Proceedings of the International Conference for High Performance Computing, Networking, Storage and Analysis*. ACM/IEEE, 2010.
- [13] Carsten Burstedde and Tobin Isaac. Morton curve segments produce no more than two distinct face-connected subdomains. *CoRR*, abs/1505.05055, 2015. <http://arxiv.org/abs/1505.05055>.
- [14] Carsten Burstedde, Lucas C. Wilcox, and Omar Ghattas. p4est: Scalable algorithms for parallel adaptive mesh refinement on forests of octrees. *SIAM Journal on Scientific Computing*, 33(3):1103–1133, 2011.
- [15] U.V. Catalyurek, E.G. Boman, K.D. Devine, D. Bozdag, R.T. Heaphy, and L.A. Riesen. Hypergraph-based dynamic load balancing for adaptive scientific computations. In *Proc. of 21st International Parallel and Distributed Processing Symposium (IPDPS’07)*. IEEE, 2007. Best Algorithms Paper Award.
- [16] Jülich Supercomputing Centre. Juqueen: Ibm blue gene/q supercomputer system at the jülich supercomputing centre. *Journal of large-scale research facilities*, 1, A1, 2015. <http://dx.doi.org/10.17815/jlsrf-1-18>.
- [17] C. Chevalier and F. Pellegrini. Pt-scotch: A tool for efficient parallel graph ordering. *Parallel Comput.*, 34(6-8):318–331, July 2008.
- [18] Willy Dorfler. A convergent adaptive algorithm for poisson’s equation. *SIAM Journal on Numerical Analysis*, 33(3):pp. 1106–1124, 1996.
- [19] Paul F. Fischer, Gerald W. Kruse, and Francis Loth. Spectral element methods for transitional flows in complex geometries. *Journal of Scientific Computing*, 17(1-4):81–98, December 2002.
- [20] N.A. Golias and R.W. Dutton. Delaunay triangulation and 3d adaptive mesh generation. *Finite Elements in Analysis and Design*, 25(3-4):331 – 341, 1997. Adaptive Meshing, Part 2.
- [21] Herman Haverkort and Freek van Walderveen. Locality and bounding-box quality of two-dimensional space-filling curves. *Computational Geometry*, 43(2):131–174, 2010.
- [22] Ø. Hjelle and M. Dæhlen. *Triangulations and Applications*. Mathematics and Visualization. Springer Berlin Heidelberg, 2006.
- [23] Tobin Isaac, Carsten Burstedde, Lucas C. Wilcox, and Omar Ghattas. Recursive algorithms for distributed forests of octrees. *SIAM Journal on Scientific Computing*, 37(5):C497–C531, 2015.
- [24] George Karypis and Vipin Kumar. A parallel algorithm for multilevel graph partitioning and sparse matrix ordering. *Journal of Parallel and Distributed Computing*, 48:71–95, 1998.
- [25] Igor Kossaczky. A recursive approach to local mesh refinement in two and three dimensions. *Journal of Computational and Applied Mathematics*, 55(3):275 – 288, 1994.
- [26] M. Lee, L. De Floriani, and H. Samet. Constant-time neighbor finding in hierarchical tetrahedral meshes. In *Shape Modeling and Applications, SMI 2001 International Conference on.*, pages 286–295, May 2001.
- [27] Anders Logg, Kent-Andre Mardal, and Garth N. Wells, editors. *Automated Solution of Differential Equations by the Finite Element Method*, volume 84 of *Lecture Notes in Computational Science and Engineering*. Springer, 2012.
- [28] G. M. Morton. A computer oriented geodetic data base; and a new technique in file sequencing. Technical report, IBM Ltd., 1966.
- [29] Leonid Oliker and Rupak Biswas. {PLUM} : Parallel load balancing for adaptive unstructured

- meshes. *Journal of Parallel and Distributed Computing*, 52(2):150 – 177, 1998.
- [30] Leonid Oliker, Rupak Biswas, and Harold N. Gabow. Parallel tetrahedral mesh adaptation with dynamic load balancing. *Parallel Comput.*, 26(12):1583–1608, November 2000.
- [31] OpenCFD. *OpenFOAM - The Open Source CFD Toolbox - User's Guide*. OpenCFD Ltd., United Kingdom, 1.4 edition, 11 April 2007.
- [32] Ekow J. Otoo and Hongwen Zhu. Indexing on spherical surfaces using semi-quadcodes. In David Abel and Beng Chin Ooi, editors, *Advances in Spatial Databases*, volume 692 of *Lecture Notes in Computer Science*, pages 510–529. Springer Berlin Heidelberg, 1993.
- [33] Guiseppe Peano. Sur une courbe, qui remplit toute une aire plane. *Math. Ann.*, 36(1):157–160, 1890.
- [34] John R. Pilkington and Scott B. Baden. Partitioning with spacefilling curves. Technical report, Dept. of Computer Science and Engineering, University of California, San Diego, 1994.
- [35] Abtin Rahimian, Ilya Lashuk, Shravan Veerapaneni, Aparna Chandramowlishwaran, Dhairya Malhotra, Logan Moon, Rahul Sampath, Aashay Shringarpure, Jeffrey Vetter, Richard Vuduc, et al. Petascale direct numerical simulation of blood flow on 200k cores and heterogeneous architectures. In *Proceedings of the 2010 ACM/IEEE International Conference for High Performance Computing, Networking, Storage and Analysis*, pages 1–11. IEEE Computer Society, 2010.
- [36] M. Rasquin, C. Smith, K. Chitale, E.S. Seol, B.A. Matthews, J.L. Martin, O. Sahni, R.M. Loy, M.S. Shephard, and K.E. Jansen. Scalable implicit flow solver for realistic wing simulations with flow control. *Computing in Science Engineering*, 16(6):13–21, Nov 2014.
- [37] Werner C. Rheinboldt and Charles K. Mesztenyi. On a data structure for adaptive finite element mesh refinements. *ACM Transactions on Mathematical Software*, 6(2):166–187, 1980.
- [38] Hans Sagan. *Space-Filling Curves*. Springer, 1994.
- [39] Jonathan Shewchuk. *Delaunay Refinement Mesh Generation*. PhD thesis, Carnegie Mellon University, Pittsburgh, May 1997. CMU CS Tech Report CMU-CS-97-137.
- [40] Jonathan Richard Shewchuk. Triangle: Engineering a 2D quality mesh generator and delaunay triangulator. In Ming C. Lin and Dinesh Manocha, editors, *Applied Computational Geometry: Towards Geometric Engineering*, volume 1148 of *Lecture Notes in Computer Science*, pages 203–222. Springer-Verlag, 1996. From the First ACM Workshop on Applied Computational Geometry.
- [41] Hang Si. *TetGen—A Quality Tetrahedral Mesh Generator and Three-Dimensional Delaunay Triangulator*. Weierstrass Institute for Applied Analysis and Stochastics, Berlin, 2006.
- [42] Wacław Sierpiński. Sur une nouvelle courbe continue qui remplit toute une aire plane. *Bulletin de l'Académie des Sciences de Cracovie*, Séries A:462 – 478, 1912.
- [43] C.W. Smith, M. Rasquin, D. Ibanez, K.E. Jansen, and M.S. Shephard. Application specific mesh partition improvement. *SIAM Journal on Scientific Computing*, 2015.
- [44] David A Steinman, Jaques S Milner, Chris J Norley, Stephen P Lownie, and David W Holdsworth. Image-based computational simulation of flow dynamics in a giant intracranial aneurysm. *American Journal of Neuroradiology*, 24(4):559–566, 2003.
- [45] James R. Stewart and H. Carter Edwards. A framework approach for developing parallel adaptive multiphysics applications. *Finite Elements in Analysis and Design*, 40(12):1599–1617, 2004.
- [46] Hari Sundar, Rahul Sampath, and George Biros. Bottom-up construction and 2:1 balance refinement of linear octrees in parallel. *SIAM Journal on Scientific Computing*, 30(5):2675–2708, 2008.
- [47] T. J. Tautges, R. Meyers, K. Merkley, C. Stimpson, and C. Ernst. MOAB: a mesh-oriented database. SAND2004-1592, Sandia National Laboratories, April 2004. Report.
- [48] Tiankai Tu, David R. O'Hallaron, and Omar Ghattas. Scalable parallel octree meshing for terascale applications. In *SC '05: Proceedings of the International Conference for High Performance Computing, Networking, Storage, and Analysis*. ACM/IEEE, 2005.
- [49] Tobias Weinzierl and Miriam Mehl. Peano—a traversal and storage scheme for octree-like adaptive Cartesian multiscale grids. *SIAM Journal on Scientific Computing*, 33(5):2732–2760, October 2011.
- [50] S. Zhang. Successive subdivisions of tetrahedra and multigrid methods on tetrahedral meshes. *Houston Journal of Mathematics*, 21(3), 1995.
- [51] Gerhard W. Zumbusch. Load balancing for adaptively refined grids. *Proceedings in Applied Mathematics and Mechanics*, 1(1), 2002.